Inorg. Chem. **2008**, *47*, 9965−9978

Persistent Radicals of Trivalent Tin and Lead

Marco Becker,[†] Christoph Förster,[†] Christian Franzen,[†] Johannes Hartrath,[†] Enzio Kirsten,[†] Jörn Knuth,[†] Karl W. Klinkhammer,*[,†] Ajay Sharma,[‡] and Dariush Hinderberger*[,‡]

Institut für Anorganische and Analytische Chemie, Johannes Gutenberg-Universität Mainz, Duesbergweg 10−14, 55128 Mainz, Germany, and Max-Planck-Institut für Polymerforschung, Ackermannweg 10, 55128 Mainz, Germany

Received June 28, 2008

In this report we present synthetic, crystallographic, and new electron paramagnetic resonance (EPR) spectroscopic work that shows that the synthetic route leading to the recently reported, first persistent plumbyl radical •$PbEbt_3$ (Ebt = ethylbis(trimethylsilyl)silyl), that is, the oxidation of the related $PbEbt_3$-anion, was easily extended to the synthesis of other persistent molecular mononuclear radicals of lead and tin. At first, various novel solvates of homoleptic potassium metallates $KSnHyp_3$ (**4a**), $KPbHyp_3$ (**3a**), $KSnEbt_3$ (**4b**), $KPbIbt_3$ (**3c**), and $KSnIbt_3$ (**4c**) (Hyp = tris(trimethylsilyl)silyl, Ibt = isopropylbis(trimethylsilyl)silyl), as well as some heteroleptic metallates, such as $[Li(OEt_2)_2][Sn^nBuHyp_2]$ (**3d**), $[Li(OEt_2)_2][Pb^nBuHyp_2]$ (**4d**), $[Li(thf)_4][PbPhHyp_2]$ (**3e**), and $[K(thf)_7][PbHyp_2\{N(SiMe_3)_2\}]$ (**3f**), were synthesized and crystallographically characterized. Through oxidation by tin(II) and lead(II) bis(trimethylsilyl)amides or the related 2,6-di-*tert*-butylphenoxides, they had been oxidized to yield in most cases the corresponding radicals. Five novel persistent homoleptically substituted radicals, that is, •$SnHyp_3$ (**2a**), •$PbHyp_3$ (**1a**), •$SnEbt_3$ (**2b**), •$SnIbt_3$ (**2c**), and •$PbIbt_3$ (**1c**), had been characterized by EPR spectroscopy. The stannyl radicals **2a** and **2c** as well as the plumbyl radical **1c** were isolated as intensely colored crystalline compounds and had been characterized by X-ray diffraction. Persistent heteroleptically substituted radicals such as •$PbHyp_2Ph$ (**1e**) or •$PbHyp_2Et$ (**1g**) had also been generated, and some selected EPR data are given for comparison. The plumbyl radicals •PbR_3 exhibit a clean monomolecular decay leading to the release of a temperature-dependent stationary concentration of branched silyl radicals. They may thus serve as tunable sources of these reactive species that may be utilized as reagents for mild radical silylations and/or as initiators for radical polymerizations. We present EPR-spectroscopic investigations for the new tin- and lead-containing compounds giving detailed insights into their electronic and geometric structure in solution, as well as structural studies on the crystalline state of the radicals, some of their anionic precursors, and some side-products.

Introduction

Recently, we reported the synthesis of the first stable plumbyl radical •$PbEbt_3$ (**1b**, Ebt = ethylbis(trimethylsilyl)-silyl).[1] It had been obtained through oxidation of the silyl-substituted potassium plumbanide $KPbEbt_3$ (**3b**) by molecular lead(II) salts. Analogous reactions had been utilized shortly before by Sekiguchi et al. in the synthesis of the homologous series •$E(SitBu_2Me)_3$ of silyl (E = Si), germyl (E = Ge), and stannyl (E = Sn) radicals.[2] However, persistent or stable mononuclear radicals of all heavier tetrels[3] but the heaviest congener lead have been known for more than 30 years.[4] Starting with the pioneering work of Lappert and co-workers

* To whom correspondence should be addressed. E-mail: hinderberger@mpip-mainz.mpg.de (D.H.), klink@uni-mainz.de (K.W.K.).
[†] Johannes Gutenberg-Universität Mainz.
[‡] Max-Planck-Institut für Polymerforschung.

(1) (a) Förster, C.; Klinkhammer, K. W.; Tumanskii, B.; Krüger, H.-J.; Kelm, H. *Angew. Chem.* **2007**, *119*, 1174–1177. (b) *Angew. Chem., Int. Ed.* **2007**, *46*, 1156−1159.

(2) (a) Sekiguchi, A.; Fukawa, T.; Nakamoto, M.; Lee, V. Ya.; Ichinohe, M. *J. Am. Chem. Soc.* **2002**, *124*, 9865. (b) Sekiguchi, A.; Fukawa, T.; Lee, V. Ya.; Nakamoto, M. *J. Am. Chem. Soc.* **2003**, *125*, 9250. (c) Chrostowska, A.; Dargelos, A.; Graciaa, A.; Baylère, P.; Lee, V. Ya.; Nakamoto, M.; Sekiguchi, A. *Organometallics* **2008**, *27*, 2915. (d) For a recent review, see Inoue, S.; Ichinohe, M.; Sekiguchi, A. *Organometallics* **2008**, *27*, 1358.

(3) The term "tetrels" had been suggested by the IUPAC as common name for the elements of group 14. To avoid terms such as "anions of the elements of group 14", it will be used together with derived denominations for derivatives such as tetryls (ER_3), tetrelanes (ER_4), or tetrelanides (MER_3) throughout this article.

(4) For recent reviews, see (a) Power, P. P. *Chem. Rev.* **2003**, *103*, 789. (b) Lee, V. Y.; Sekiguchi, A. *Eur. J. Inorg. Chem.* **2005**, 1209.

10.1021/ic801198p CCC: $40.75
Published on Web 09/30/2008

who synthesized radicals such as •E[N(SiMe$_3$)$_2$]$_3$ or •E[CH(SiMe$_3$)$_2$]$_3$,[5] such radicals have been the subject of several papers in the last three decades. In the 1990s a revival of radical chemistry of group 14 had been observed. Several oligonuclear radicals with varying degree of delocalization of the unpaired electron had been prepared since then.[6]

Our early electron paramagnetic resonance (EPR) measurements on the mononuclear plumbyl radical **1b** in solution revealed strong, broad, and structureless resonances for **1b** at a *g* value markedly larger than for all related radicals of the lighter congeners in group 14.[1] A second signal was present at even higher *g*-values. It was at first attributed to a second, lead-centered radical species. The expected satellite pattern according to hyperfine-coupling within the isotopomer ^{207}PbEbt$_3$ could not readily be found, however. Therefore, we at first proposed a very large hyperfine-coupling constant for this isotopomer lying outside the range of the employed spectrometer. In this report we present a detailed analysis of new EPR data of **1b** which reveals that the second signal does not derive from a further radical species but is part of the low-field manifold of the ^{207}Pb hyperfine splitting pattern. Additionally, we present synthetic and analytic work that shows that the synthetic route mentioned above, that is, the oxidation of appropriate tetrel anions, may easily be extended to the synthesis of further related persistent homoleptic molecular radicals of lead and tin: •PbHyp$_3$ (**1a**), •PbIbt$_3$ (**1c**), •SnHyp$_3$ (**2a**), •SnEbt$_3$ (**2b**), and •SnIbt$_3$ (**2c**) (Hyp = Si(SiMe$_3$)$_3$, Ibt = isopropylbis(trimethylsilyl)silyl), and by slight modifications may also give access to related heteroleptic species such as SnHyp$_2$Ph and PbHyp$_2$Ph. We furthermore present detailed continuous wave EPR (CW EPR) and low-temperature, echo-detected EPR data on the four selected persistent molecular tetryl radicals **1a**, **1b**, **2a**, and **2c**, (see Figure 1) which allow the characterization of the structure and dynamics of these molecules in fluid and frozen solution.

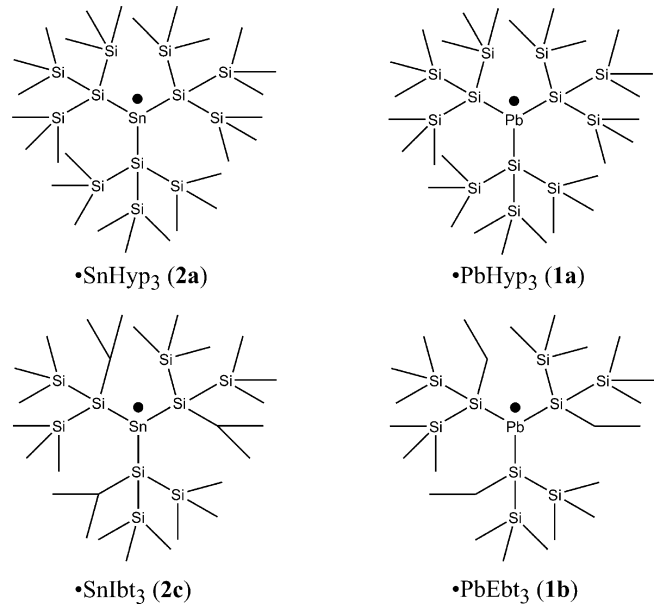

Figure 1. Molecular structures of the four persistent or stable lead- and tin based radicals that were characterized in detail using EPR spectroscopy.

Experimental Section

Syntheses. Preparation of Compounds. Reactions were performed under an argon atmosphere using standard Schlenk lines, and the resulting air-sensitive compounds were manipulated under nitrogen atmosphere within a drybox. Syntheses of the potassium salts KHyp, KEbt, and KIbt, as well as those of the molecular Sn(II) and Pb(II) precursors Sn[N(SiMe$_3$)$_2$]$_2$, Pb[N(SiMe$_3$)$_2$]$_2$, SnHyp$_2$ (**5**), and PbHyp$_2$ (**6**), were carried out as reported previously.[7−10] Diethyl ether and pentane were distilled from LiAlH$_4$. Toluene and tetrahydrofuran were distilled from Na/benzophenone. All solvents were stored under Ar over 3 Å molecular sieves. All other reagents not mentioned in the following were synthesized by procedures according to the literature or purchased and used without further purification.

Sn(OC$_6$H$_3$^{t}Bu$_2$-2,6)$_2$ and Pb(OC$_6$H$_3$^{t}Bu$_2$-2,6)$_2$.[11] To a 350 mL *n*-pentane solution of Sn[N(SiMe$_3$)$_2$]$_2$ (16.66 g, 37.9 mmol) or Pb[N(SiMe$_3$)$_2$]$_2$ (20.01 g, 37.9 mmol) was added 2,6-di-*tert*-butylphenol (15.64 g, 75.8 mmol), and the resulting yellow (Sn) or orange (Pb) suspension was stirred overnight. The solid was separated by filtration through a sintered glass filter (G4), washed three times with 20 mL of toluene and subsequently dried in dynamic vacuum. The products are obtained as bright yellow or orange powder in yields of 92 and 94%, respectively and are only sparingly soluble in organic solvents.

Sn(OC$_6$H$_3$^{t}Bu$_2$-2,6)$_2$. Anal. Calcd for C$_{28}$H$_{42}$O$_2$Sn: C, 63.53; H, 8.00. Found: C, 63.64; H, 8.12. ^{1}H NMR (C$_6$D$_6$): δ 7.48 (d, 4H), 6.74 (t, 2H), 1.62 (s, 18H).

Pb(OC$_6$H$_3$^{t}Bu$_2$-2,6)$_2$. Anal. Calcd for C$_{28}$H$_{42}$O$_2$Pb: C, 54.43; H, 6.85. Found: C, 54.56; H, 6.96. ^{1}H NMR (C$_6$D$_6$): δ 7.36 (d, 4H), 6.90 (t, 2H), 1.58 (s, 18H).

[Li(thf)$_4$][PhHyp$_2$Pb] (3e). To a stirred yellow 10 mL di-*n*-butylether solution of phenyllithium (1.91 mmol) at 0 °C was added quickly a green 6 mL solution of **6** (1.34 g, 1.91 mmol) in diethyl

(5) See, for example, (a) Davidson, P. J.; Hudson, A.; Lappert, M. F.; Lednor, P. W. *J. Chem. Soc., Chem. Commun.* **1973**, 829. (b) Cotton, J. D.; Cundy, C. S.; Harris, D. H.; Hudson, A.; Lappert, M. F.; Lednor, P. W. *J. Chem. Soc., Chem. Commun.* **1974**, 651. (c) Lappert, M. F.; Lednor, P. W. *Adv. Organomet. Chem.* **1976**, *14*, 345. (d) Hudson, A.; Lappert, M. F.; Lednor, P. W. *J. Chem. Soc., Dalton Trans.* **1976**, 2369.

(6) See, for example, (a) Olmstead, M. M.; Pu, L.; Simons, R. S.; Power, P. P. *Chem. Commun.* **1997**, 1595. (b) Olmstead, M. M.; Simons, R. S.; Power, P. P. *J. Am. Chem. Soc.* **1997**, *119*, 11705. (c) Pu, L.; Haubrich, S. T.; Power, P. P. *J. Organomet. Chem.* **1999**, *582*, 100.

(7) Harris, D. H.; Lappert, M. F. J. *Chem. Soc., Chem. Commun.* **1974**, 895.

(8) Marschner, C. *Eur. J. Inorg. Chem.* **1998**, 221.

(9) Kayser, C.; Fischer, R.; Baumgartner, J.; Marschner, C. *Organometallics* **2002**, *21*, 1023.

(10) Klinkhammer, K. W.; Schwarz, W. *Angew. Chem., Int. Ed.* **1995**, *34*, 1334.

(11) Sn(OC$_6$H$_3$^{t}Bu$_2$-2,6) $_2$ was synthesized before in moderate yield by reaction of SnI$_4$ and KOC$_6$H$_3$^{t}Bu$_2$-2,6 (detailed procedure not given) and had been characterized crystallographically: Barnhart, D. M.; Clark, D. L.; Watkin, J. G. *Acta Cryst. C* **1994**, *50*, 702. Related tetrel aryloxides with an additional 4-Me substituent had also been described before. However, the better solubility of the corresponding alkali metal aryloxides in organic solvents, make them less suitable as oxidizers in the synthesis of tetryl radicals. For preparation and properties see: Çetinkaya, B.; Gümrükçü, I.; Lappert, M. F.; Atwood, J. L.; Rogers, R. D.; Zaworotko, M. J. *J. Am. Chem. Soc.* **1980**, *102*, 2086. Çetinkaya, B.; Gümrükçü, I.; Lappert, M. F.; Atwood, J. L.; Shakir, R. *J. Am. Chem. Soc.* **1980**, *102*, 2088.

ether (prepared at −60 °C). The resulting orange solution was evaporated to dryness, and the obtained solid was redissolved in 2 mL of tetrahydrofuran. After storing at −60 °C for 18 h crystalline yellow plumbanide **3e** was isolated in 88% yield. ^{1}H NMR (C_6D_6): δ 8.75 (d, 2H), 7.12 (t, 2H), 7.01 (t, 1H), 0.50 (d, 4H); ^{13}C NMR (C_6D_6): 123.3, 127.8, 147.5, 5.8; ^{29}Si NMR (C_6D_6): −122.9 (*Si*Si$_3$), −4.8 (*Si*Me$_3$).

Li(thf)$_2$SnHyp$_2$^{n}Bu (4d) and Li(thf)$_2$PbHyp$_2$^{n}Bu (3d). A 0.5 mL portion of a 2.0 M solution of *n*-butyllithium in *n*-hexane was added at −60 °C to 10 mL of diethyl ether. Under intense stirring, a precooled 5 mL dark brown (respectively blue) solution of **5** in *n*-pentane (0.71 g, 1 mmol) (respectively **6** (0.65 g, 1 mmol) was quickly added to this mixture, and an immediate color change to yellow (respectively orange) was observed. After evaporating to dryness the resulting solid was recrystallized from *n*-pentane. The lithium stannanide **4d** (respectively plumbanide **3d**) was obtained as a pale yellow (respectively orange) crystalline material in 65% (respectively 86%) yield. **4d**: ^{1}H NMR (C_6D_6): δ 3.26 (q, 8H, OC*H*$_2$CH$_3$), 1.81 (m, 2H), 1.62 (m, 2H), 1.56 (m, 2H), 1.12 (t, 3H, CH$_3$ (^{n}Bu)), 0.92 (t, 12H, OCH$_2$C*H*$_3$), 0.51 (s, 54H, *Hyp*); ^{13}C NMR (C_6D_6): 65.2 (Et$_2$O), 39.0, 30.1, 14.5 (Et$_2$O), 14.1, 5.9 (*Hyp*); ^{29}Si NMR (C_6D_6): −142.1 (*Si*Si$_3$), −7.2 (*Si*Me$_3$ [$^1J_{SiC}$ 42.1 Hz]); ^{119}Sn-NMR (C_6D_6): −345 [$^1J_{LiSn}$ 534 Hz]; ^{7}Li NMR (C_6D_6): 0.54. **3d**: ^{1}H NMR (C_6D_6): δ 3.22 (q, 8H, OC*H*$_2$CH$_3$), 2.22 (m, 2H), 2.05 (m, 2H), 1.60 (m, 2H), 1.15 (t, 3H), 0.94 (t, 12H, OCH$_2$C*H*$_3$), 0.55 (s, 54H, *Hyp*); ^{13}C NMR (C_6D_6): 65.1 (Et$_2$O), 40.2, 32.4, 14.9 (Et$_2$O), 13.9, 6.9 (*Hyp*); ^{29}Si NMR (C_6D_6): −142.6 (*Si*Si$_3$), −5.4 (*Si*Me$_3$ [$^1J_{SiC}$ 42.1 Hz]);^{7}Li NMR (C_6D_6): 1.36.

General Procedure for the Generation of Heteroleptic Stannyl and Plumbyl Radicals •EHyp$_2$R. A solution of 2 mmol of the stannylene **5** or the plumbylene **6** in 10 mL of *n*-pentane, respectively, was added to about 15 mL solution of 1.1 equiv of the appropriate hydrocarbyllithium at −80 °C. This had been freshly prepared by mixing the commercial available alkane or ether solution (approximately 1−2 mol/L) with 10 mL of precooled tetrahydrofuran. Under intense stirring, the solution was allowed to warm to room temperature and kept at 20 °C for 1 h. After filtering out the precipitate, the resulting solution was treated with 0.55 equiv of solid Pb[OC$_6$H$_3$$tBu_2$-2,6]$_2$, giving a deeply colored solution of the desired radical, which could be identified by its EPR signals. ^{1}H NMR spectra recorded on this solution generally show the presence of varying amounts of diamagnetic byproducts.

General Procedure for the Synthesis of the Homoleptic Tetrelanides KE[SiR(SiMe$_3$)$_2$]$_3$ 3b, 3c, 4b, and 4c. An equimolar mixture of the appropriate silane SiR(SiMe$_3$)$_3$ (20 mmol) and KO^{t}Bu (20 mmol) was dissolved in 100 mL of tetrahydrofuran and stirred for 12 h. The resulting yellow or orange solution was evaporated to dryness and heated in dynamic vacuum to 30−40 °C for 1d. The residue was then dissolved in diethyl ether, cooled to −60 °C, and a suspension of E(OAr*)$_2$ (6.67 mmol) in 100 mL of diethyl ether was added slowly during 3 h. The yellow to red reaction mixture was stirred for an hour at −30 °C and afterward filtered at −50 °C. The volume of the filtrate was reduced to about 10 mL at −50 °C, and 20 mL of *n*-pentane was added. After 2 d at −60 °C the tetrelanide had precipitated as a yellow to red crystalline material (67−85% overall yield). Additional amounts of the tetrelanide may be obtained from the mother liquor by repeated concentration and cooling.

3b: K(OEt$_2$)$_2$Pb[SiEt(SiMe$_3$)$_2$]$_3$: 72% yield; ^{1}H NMR (C_6D_6): δ 3.16 (q, 8H, OC*H*$_2$CH$_3$), 1.44 (m, 6H), 1.35 (t, 9H), 1.00 (t, 12H, OCH$_2$C*H*$_3$), 0.48 (s, 18H, *SiMe*$_3$); ^{13}C NMR (C_6D_6): 65.8 (O*C*H$_2$CH$_3$), 17.8 (PbCH$_2$*C*H$_3$), 15.4 (OCH$_2$*C*H$_3$), 11.2 (Pb*C*H$_2$-*C*H$_3$), 4.0 (SiMe$_3$ [$^1J_{SiC}$ 41.1 Hz]); ^{29}Si NMR (C_6D_6): −78.2 (*Si*Si$_3$ [$^1J_{PbSi}$ 1378 Hz]), −9.6 (*Si*Me$_3$ [$^2J_{PbSi}$ 20.4 Hz]); ^{207}Pb-NMR (C_6D_6): −1119.8.

3c: K(OEt$_2$)$_2$Pb[Si^{i}Pr(SiMe$_3$)$_2$]$_3$: 67% yield; ^{1}H NMR (C_6D_6): δ 3.14 (q, 8H, OC*H*$_2$CH$_3$), 1.48 (d, 18H), 1.04 (sept, 3H), 1.01 (t, 12H, OCH$_2$C*H*$_3$), 0.51 (s, 18H, *SiMe*$_3$); ^{29}Si NMR (C_6D_6): −79.3 (*Si*Si$_3$ [$^1J_{PbSi}$ 1378 Hz]), −9.3 (*Si*Me$_3$).

4b: K(OEt$_2$)$_3$Sn[SiEt(SiMe$_3$)$_2$]$_3$: 85% yield; ^{1}H NMR (C_6D_6): δ 3.14 (q, 12H, OC*H*$_2$CH$_3$), 1.22 (q, 6H), 1.03 (t, 9H), 1.02 (t, 18H, OCH$_2$C*H*$_3$), 0.41 (s, 18H, *SiMe*$_3$); ^{29}Si NMR (C_6D_6): −76.1 (*Si*Si$_3$ [$^1J_{PbSi}$ 1378 Hz]), −11.0 (*Si*Me$_3$); ^{119}Sn-NMR (C_6D_6): −702.6.

4c: K(OEt$_2$)$_2$Sn[Si^{i}Pr(SiMe$_3$)$_2$]$_3$: 79% yield; ^{1}H NMR (C_6D_6): δ 3.16 (q, 8H, OC*H*$_2$CH$_3$), 1.44 (d, 18H), 1.67 (sept, 3H), 1.01 (t, 12H, OCH$_2$C*H*$_3$), 0.50 (s, 18H, *SiMe*$_3$); ^{13}C NMR (C_6D_6): 65.8 (O*C*H$_2$CH$_3$), 25.6 (PbCH$_2$*C*H$_3$), 15.4 (OCH$_2$*C*H$_3$), 4.7 (SiMe$_3$); ^{29}Si NMR (C_6D_6): −63.5 (*Si*Si$_3$), −10.7 (*Si*Me$_3$).

(OEt$_2$)$_2$KPbHyp$_3$ (3a′) and [K(thf)$_6$][PbHyp$_3$] (3a″). Solvent-free KHyp (1.43 g, 5 mmol) was suspended in 10 mL of *n*-pentane and cooled to −60 °C. Then 10 mL of diethyl ether was added. A cooled (−60 °C) 15 mL *n*-pentane solution of **6** (3.56 g, 5 mmol) was slowly added to the KHyp suspension, and a color change to red-violet as well as precipitation of a violet solid was observed. The reaction mixture was stirred for 2 h, and the cold solution evaporated to dryness. The obtained solid was recrystallized from *n*-pentane. **3a′** was isolated as red-violet platelets in 89% yield. Recrystallization from tetrahydrofuran or direct synthesis in this solvent yielded the thf-solvate **3a″** as violet rod-shaped crystals in 86% yield.

3a′: ^{1}H NMR (C_6D_6): δ 3.21 (q, 8H, OC*H*$_2$CH$_3$), 1.05 (t, 12H, OCH$_2$C*H*$_3$), 0.57 (s, 18H, *SiMe*$_3$); ^{13}C NMR (C_6D_6): 65.9 (O*C*H$_2$-CH$_3$), 14.2 (OCH$_2$*C*H$_3$), 4.6 (SiMe$_3$); ^{29}Si NMR (C_6D_6): −129.9 (*Si*Si$_3$), −9.5 (*Si*Me$_3$).

[K(thf)$_6$][SnHyp$_3$] (4a″) and [K(thf)$_4$(C$_6$H$_6$)$_2$][K(SnHyp$_3$)$_2$] (4a‴). To a 20 mL diethyl ether solution of KHyp (0.315 g, 1.1 mmol) was slowly added a 10 mL diethyl ether solution of **5** (0.713 g, 1.1 mmol) at −60 °C. The brown solution was stirred for 2 h at −60 °C and further 15 min at room temperature. After concentration in vacuum to a volume of 5 mL, tetrahydrofurane (2 mL) was added. Storing at −60 °C for 2 d afforded needle-shaped orange crystals of **4a″** in 65% yield.

Thorough drying of **4a″** for 12 h at 30 °C and subsequent recrystallization from a saturated benzene solution (25°/6 °C) finally gave orange platelets of the potassiate **4a‴**.

4a″: ^{1}H NMR (C_6D_6): δ 0.55 (s, 81H, *SiMe*$_3$); ^{13}C NMR (C_6D_6): 7.2 (SiMe$_3$); ^{29}Si NMR (C_6D_6): −134.1 (*Si*Si$_3$), −7.2 (*Si*Me$_3$).

4‴: ^{1}H NMR (C_6D_6): δ 0.53 (s, 81H, *SiMe*$_3$); ^{13}C NMR (C_6D_6): 6.9 (SiMe$_3$); ^{29}Si -NMR (C_6D_6): −132.3 (*Si*Si$_3$), −7.5 (*Si*Me$_3$).

[K(thf)$_7$][PbHyp$_2${N(SiMe$_3$)$_2$}] (3f). Twelve milliliters of a solution of KN(SiMe$_3$)$_2$ (0.31 g, 1.54 mmol) in a 5:1 mixture of tetrahydrofuran and diethyl ether was added to a green 5 mL diethyl ether solution of **6** (1.10 g, 1.54 mmol) at −60 °C, resulting in an immediate color change to red-brown. After 2 h the solution was warmed to room temperature and stirred for an additional 15 min. After solvent reduction to 5 mL and storing at −60 °C for 2 d, **3f** had been obtained as red platelets (85% yield), which, however, proved not suitable for X-ray analysis. A suitable red single crystalline block was finally obtained by recrystallization from toluene.^{1}H NMR (C_6D_6): δ 3.52 (m, thf), 1.40 (m, thf), 0.41 (s, Hyp), 0.17 (s, N(SiMe$_3$)$_2$); ^{13}C NMR (C_6D_6): 68.3 (thf), 25.8 (thf),

8.3 (Hyp), 7.2 ($N(SiMe_3)_2$); ^{29}Si NMR (C_6D_6): −31.6 ($SiSi_3$), −20.1 (NSi_2), 7.9 ($SiSi_3$). UV−vis (*n*-pentane): 238 (sh, 3.09×10^4), 303 (sh, 1.36×10^4), 341 (sh, 5.96×10^3), 455 (1.61×10^3).

•SnHyp$_3$ (2a). 2a was either synthesized by oxidation of pure stannanide **4a** or preferably in a one-pot fashion without isolating **4a** prior to oxidation. The latter procedure started from a 10 mL diethyl ether solution of solvated KHyp ($K(thf)_{0.8}Hyp$, 1.53 g, 4.44 mmol). A suspension of $Sn(OC_6H_3{}^tBu_2\text{-}2,6)_2$ (0.87 g, 1.64 mmol) in 10 mL of diethyl ether was added to the KHyp solution in four portions during 2 h at −60 °C. The resulting orange-red mixture was warmed to −30 °C and stirred for another 30 min. Then again 10 mL of a suspension of $Sn(OC_6H_3{}^tBu_2\text{-}2,6)_2$ (0.42 g, 0.80 mmol) in diethyl ether was added in four portions at −60 °C during 1 h. The resulting dark brown mixture was warmed to −30 °C and stirred for 45 min. After subsequent cooling to −60 °C it was filtered and the filtrate was concentrated at −50 °C in a dynamic vacuum to 10 mL. From this solution very pure **2a** was isolated by crystallization at −60 °C for 2 d in 49% yield (0.7 g 0.81 mmol). UV−vis (*n*-pentane): 343 (1.46×10^3), 457 (sh, 100).

Generation of •PbHyp$_3$ (1a). Five milliliters of an *n*-pentane solution of $Pb[N(SiMe_3)_2]_2$ (0.46 g, 0.88 mmol) was added to a 20 mL tetrahydrofuran solution of $(OEt_2)_2KPbHyp_3$ (**3a′**) (2 g, 1.76 mmol) at −60 °C and stirred for 2 h. After filtration at −60 °C the mixture was concentrated to 5 mL in a dynamic vacuum at −20 °C. By storing at −60 °C for 1 week most of the formed $PbHyp_2$ (**6**) was isolated as the blue-green thf-solvate Hyp_2Pb•thf (**6a**) and plumbanide **3f**. EPR experiments on the dark green mother liquor prove the presence of significant amounts of **1a**. By NMR, further **6**, the octasilane Hyp_2, and small amounts of $KN(SiMe_3)_2$ could be detected as diamagnetic contaminations.

•SnEbt$_3$ (2b), •SnIbt$_3$ (2c), and •PbIbt$_3$ (1c). Solid $Sn(OC_6H_3{}^tBu_2\text{-}2,6)_2$ (2.65 g, 5 mmol) or $Pb(OC_6H_3{}^tBu_2\text{-}2,6)_2$ (3.08 g, 5 mmol) was added to a 50 mL diethyl ether solution of stannanide **4b** (10 mmol), stannanide **4c** (10 mmol), or plumbanide **3c** (10 mmol) at −60 °C, respectively. The reaction mixture was stirred at −60 °C for 1 h and at −30 °C for 30 min. The resulting brown-red (**2b** and **2c**) or brown-green suspensions (**1c**) were filtered at −30 °C, and the filtrates were concentrated to 5 mL in a dynamic vacuum. After storing at −60 °C for 2 weeks (**2c**) or 2 days (**1c**), the respective radicals **2c** and **1c** could be isolated as large orange-yellow or small green platelets in 65% and 43% yield, while $•Sn_3Ebt$ (**2b**) did not crystallize, but was isolated as an orange-yellow oil (approximately 70% yield). Very small black crystals of the *hexaprisma*-hexastannane **7** were embedded within the crystals of **2c**.

X-ray Crystallographic Study. All crystals were covered with inert oil at −50 °C and mounted to a nylon loop using an X-TEMP 2 system.[12] They were then transferred to the diffractometer under permanent cooling. X-ray diffraction experiments were carried out on a Bruker SMART CCD diffractometer using Mo Kα radiation ($\lambda = 0.71073$ Å). Data were collected at −80 or −100 °C with a frame width of 0.5° either in ω or in ϕ. The diffraction frames were integrated using the SAINT package and most were corrected for absorption with MULABS.[13,14] The structures were solved by direct methods and refined by the full-matrix method based on F^2 using the SHELXTL software package.[15]

(12) Kottke, T.; Stalke, D. *J. Appl. Crystallogr.* **1993**, *26*, 615–619.
(13) *SMART Data Collection and SAINT-Plus Data Processing Software for the SMART System* (various versions); Bruker Analytical X-Ray Instruments, Inc.: Madison, WI, 2000.
(14) Blessing, B. *Acta Crystallogr.* **1995**, *A51*, 33.
(15) (a) Sheldrick, G. M. *SHELXTL*, Version 5.1; Bruker AXS: Madison, WI, 1998. (b) Sheldrick, G. M. *SHELXL-97*; University of Göttingen: Göttingen, Germany, 1997.

Scheme 1. General Synthetic Routes Leading to Alkali Metal Tetrelanides[a]

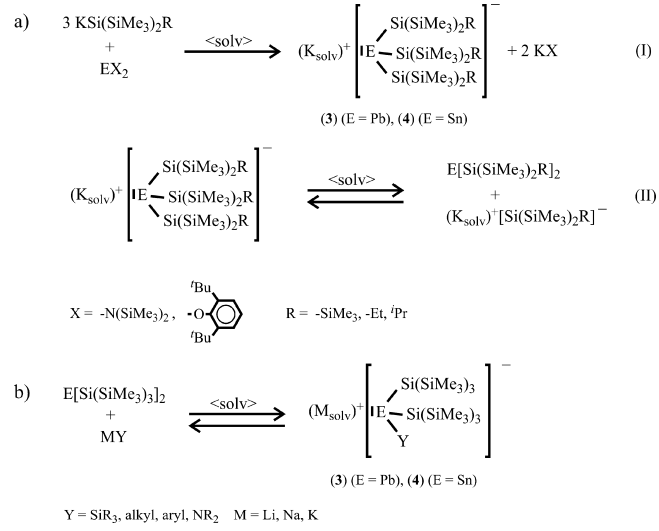

[a] (a) *homoleptic* silyl-substituted tetrelanides KER_3 (E = Sn, Pb; R = Hyp, Ebt, Ibt), i.e. the series **3a-c** and **4a-c.** $EX_2 = E[N(SiMe_3)_2]_2$ or preferably $E(OC_6H_3\text{-}{}^tBu\text{-}2,6)_2$ in aprotic coordinating solvents; (b) *heteroleptic* tetrelanides: dihypersilyltetrelandiyls $EHyp_2$ are synthesized and isolated first and then in a subsequent step are reacted with alkali metal hydrocarbyls or other alkali metal salts MY.

CCDC 692387−692399 contain the supplementary crystallographic data for this paper. These data can be obtained free of charge from The Cambridge Crystallographic Data Centre via www.ccdc.cam.ac.uk/data_request/cif. The crystal parameters and basic information related to data collection and structure refinement are, however, summarized in Tables S1−S3 in the Supporting Information.

In all of the listed compounds but hexastannane **7**, all non-hydrogen atoms were refined anisotropically while the positions of all hydrogen atoms were generated with appropriate geometric constraints and allowed to ride on their respective parent carbon atoms with fixed isotropic thermal parameters. Compound **7** had been obtained as very small crystals only ($V < 10^{-3}$ mm^3). Because of weak reflection data only the tin and silicon atoms could be refined anisotropically while the carbon atoms were refined with isotropic thermal parameters.

EPR Spectroscopy. CW EPR spectra in fluid ($T = 293$ K) solution at X-band (∼9.4 GHz) were measured either on a Bruker ELEXSYS 580 spectrometer with a rectangular cavity (4103TM, Q-values typically 3000) and an Oxford open flow cryostat cooling system or a Magnettech MiniScope MS200 benchtop CW EPR spectrometer with a variable-temperature cooling/heating finger. The tin and lead substances were dissolved in 1:1 mixtures of *n*-pentane and *n*-heptane and subsequently transferred into EPR sample tubes (quartz glass, 4 mm outer diameter tubes for the ELEXSYS 580 spectrometer, 3 mm outer diameter for the MiniScope MS200). Echo-detected, field-swept EPR spectra were recorded with a primary echo sequence ($\pi/2$)-τ-(π)-τ-echo while sweeping the magnetic field using the same Bruker ELEXSYS 580 spectrometer with a dielectric resonator (MD4EN, overcoupled to Q-values of typically 100). The temperature was set to 20 K by cooling with liquid helium using an Oxford cryostat and cooling system.

The samples were prepared as concentrated solutions (concentrations typically >10 mM) and the sample volume was always large enough to fill the complete resonator volume in the probehead (>300 μL).

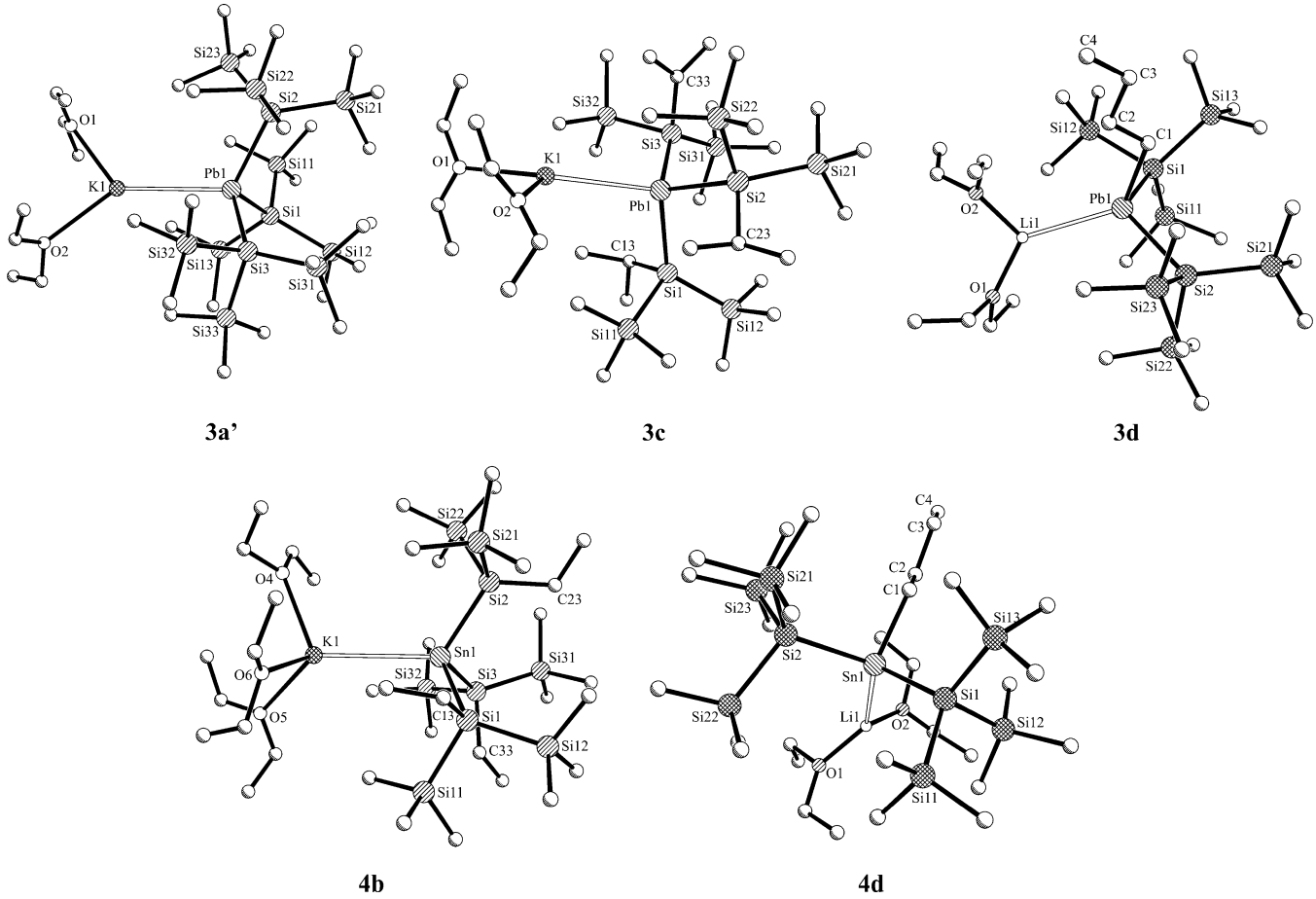

Figure 2. Molecular structures of the alkali metal tetrelanides **3a**, **3c**, **3d**, **4b**, and **4d** forming contact-ion pairs. Selected bond lengths and angles are given in [Å, deg]. $(Et_2O)_2KPbHyp_3$ (**3a′**): K1−O1 2.596(6), K1−O2a 2.683(9), Pb1−K1 3.694(2), Pb1−Si1 2.851(2), Pb1−Si2 2.809(2), Pb1−Si3 2.837(2), Si1−Pb1−Si2 106.02(7), Si1−Pb1−Si3 109.34(7), Si2−Pb1−Si3 107.98(7), Si1−Pb1−K1 113.55(6), Si2−Pb1−K1 116.37(6), Si3−Pb1−K1 103.35(6). $(Et_2O)_2KPbIbt_3$ (**3c**): K1−O2 2.60(2), K1−O1 2.77(2), Pb1−K1 3.607(4), Pb1−Si1 2.705(5), Pb1−Si2 2.722(5), Pb1−Si3 2.726(6), Si1−Pb1−Si2 105.4(2), Si1−Pb1−Si3 105.8(2), Si2−Pb1−Si3 107.9(2), Si1−Pb1−K1 110.42(15), Si2−Pb1−K1 114.04(15), Si3−Pb1−K1 112.8(2). $(Et_2O)_2LiPbnBuHyp_2$ (**3d**): Li1−O1 1.906(11), Li1−O2a 1.874(15), Pb1−Li1 2.954(10), Pb1−C1 2.323(5), Pb1−Si1 2.726(2), Pb1−Si2 2.741(2), Si1−Pb1−Si2 113.18(5), C1−Pb1−Si1 93.15(15), C1−Pb1−Si2 96.02(15), C1−Pb1−Li1 120.6(3), Si1−Pb1−Li1 115.4(2), Si2−Pb1−Li1 115.3(2). $(Et_2O)_3KSnEbt_3$ (**4b**): K1−O4 2.768(3), K1−O5 2.808(3), K1−O6 2.701(4), Sn1−K1 3.7234(9), Sn1−Si1 2.6738(8), Sn1−Si2 2.6442(8), Sn1−Si3 2.6735(9), Si2−Sn1−Si3 105.67(3), Si2−Sn1−Si1 104.82(3), Si3−Sn1−Si1 100.87(3), Si2−Sn1−K1 121.74(2), Si3−Sn1−K1 113.55(2), Si1−Sn1−K1 107.90(2). $(Et_2O)_2LiSnnBuHyp_2$ (**4d**): Li1−O1 1.909(5), Li1−O2a 1.895(11), Sn1−Li1 3.020(5), Sn1−C1 2.233(3), Sn1−Si1 2.6544(7), Sn1−Si2 2.6668(7), Si1−Sn1−Si2 114.29(2), C1−Sn1−Si1 94.15(8), C1−Sn1−Si2 97.68(9), C1−Sn1−Li1 119.88(12), Si1−Sn1−Li1 113.23(11), Si2−Sn1−Li1 115.19(10).

Data Analysis. All spectral simulations were performed with home-written programs in MATLAB (The MathWorks, Inc.) employing the EasySpin toolbox for EPR spectroscopy.[16] Simulations of CW EPR spectra in fluid solution were performed using a model, which is based on the slow-motion theory and a program developed by Schneider and Freed as implemented in EasySpin. These simulations can account for the effect of intermediate or slow rotational diffusion of the radical on the EPR spectra.[17] Low-temperature, powder-type EPR spectra were simulated by directly computing the resonance fields and transition probabilities over a triangular orientational powder grid, again as implemented in EasySpin.

The corresponding magnetic parameters (*g*- and hyperfine (*A*-) tensor elements) found from the simulations of all tin- and lead-centered radicals are given in Table 4.

(16) Stoll, S.; Schweiger, A. *J. Magn. Reson.* **2006**, *178*, 42–55; see http://www.easyspin.org.

(17) Schneider, D. J.; Freed, J. H. In *Biological Magnetic Resonance Vol.8: Spin Labeling - Theory and Applications*; Berliner, L. J., Reuben, L. J., Eds.; Plenum Press: New York, 1989.

Results and Discussion

The *homoleptic* silyl-substituted tetrelanides $KE(SiR_3)_3$ (E = Sn {**3a-c**}, Pb {**4a-c**}; R = Hyp, Ebt, Ibt) are obtained in good to excellent yields by the reaction of 3 equiv of the proper bulky alkali metal silanides with soluble lead(II) or tin(II) salts such as $E[N(SiMe_3)_2]_2$ or preferably $E(OC_6H_3\text{-}^tBu\text{-}2,6)_2$[11] in aprotic coordinating solvents (Scheme 1a). For E = Pb, the oxidation of the potassium silanide is observed as a side reaction, giving elementary lead and metal-free silanes. The latter become the predominant products if inorganic lead salts such as $PbCl_2$ are used as starting material.

In the absence of coordinating solvents or if the anion of the alkali metal silanide reaches a certain size, the equilibrium (2) in Scheme 1 (top) is markedly shifted to the left side. If very large silanide anions are introduced, plumbanides cannot be isolated any more. We have found that (from THF solution) the critical size which still allows for the isolation of solvated homoleptic potassium plumbanides is reached

Scheme 2. Generation of the Persistent or Stable Lead- and Tin-Based Radicals by Oxidation of the Alkali Metal Salts (Scheme 1) with Appropriate Oxidants (See Text for Details)[a]

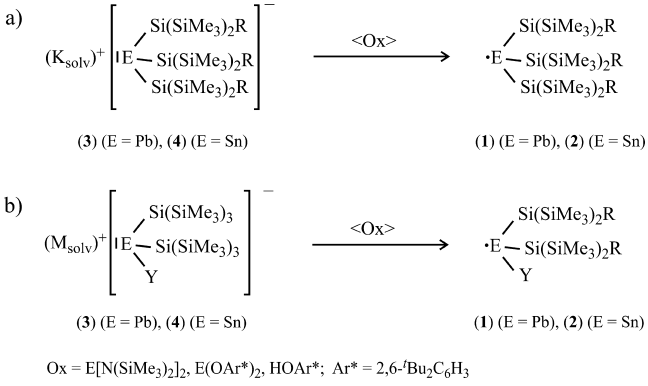

[a] Oxidation is achieved by molecular tin(II) or lead(II) salts such as $E[N(SiMe_3)_2]_2$ and $E(OAr^*)_2$ or the phenol Ar*OH (Ar* = C_6H_3-^{t}Bu$_2$-2,6); (a) *homoleptic* tetryl radicals; (b) *heteroleptic* tetryl radicals.

for the hypersilyl anion $Si(SiMe_3)_3^-$ (Hyp^-). While the respective stannanide $KSnHyp_3$ (**4a**), probably because of the stronger Sn−Si bonds, does not dissociate to $SnHyp_2$ and KHyp to a notable extent, solutions of the plumbanide $KPbHyp_3$ (**3a**) exhibit broad ^{1}H- and ^{13}C NMR resonances with chemical shifts markedly depending on the concentration, and in the solid-state structure of the solvate $(Et_2O)_2$-$KPbHyp_3$ (**3a′**, Figure 2) very long Pb−Si bonds are observed. Replacing one of the nine methyl groups of the hypersilyl substituent for a *tert*-butyl group completely prevents the formation of the respective plumbanide. Instead, unreacted $Pb[Si(Si^tBuMe_2)(SiMe_3)_2]_2$ and $K[Si(Si^tBuMe_2)$-$(SiMe_3)_2]$ are detected as the predominant species in solution by ^{1}H-, ^{13}C-, and ^{29}Si NMR experiments.[18]

Heteroleptic tetrelanides are also available if bis(silyl)tetrelandiyls are synthesized and isolated first and are then in a subsequent step reacted with alkali metal hydrocarbyls or other alkali metal salts (Scheme 1b). Following this route, we were able to isolate several unsymmetrically substituted tetrelanides bearing two hypersilyl groups and an alkyl, aryl, or amido substituent. The synthesis is obviously restricted to systems where the respective bis(silyl)tetrelandiyl possesses a sufficient kinetic stability to allow for its isolation. Dihypersilyltetrelandiyls, $SnHyp_2$ (**5**; as the dimer $\mathbf{5}_2$) and $PbHyp_2$ (**6**),[10] are such species of sufficient stability and can therefore be used for the synthesis of a range of heteroleptic hypersilyl-substituted tetrelanides such as **3d**, **3e**, **3f**, and **4d**. However, heteroleptic derivatives comprising less demanding groups such as ethylbis(trimethylsilyl)silyl (Ebt) are hitherto unknown, because tetrelandiyls such as Ebt_2E are not accessible under the conditions used for the preparation of the hypersilyl derivatives **5** and **6**.

The next step to tetryl radicals would be the oxidation of the alkali metal salts with appropriate oxidants (Scheme 2). We found that molecular tin(II) or lead(II) salts such as $E[N(SiMe_3)_2]_2$ or $E(OC_6H_3$-^{t}Bu$_2$-2,6)$_2$ can be used. Since the alkali metal salts of 2,6-di-*tert*-butylphenol exhibit very low solubility in weakly polar solvents and may thus be easily

(18) Förster, C.; Klinkhammer, K. W., to be published.

Scheme 3. Formation and Decay of the Hypersilyl-Based Lead Radical **1a** As Corroborated by Chemical and NMR Analysis

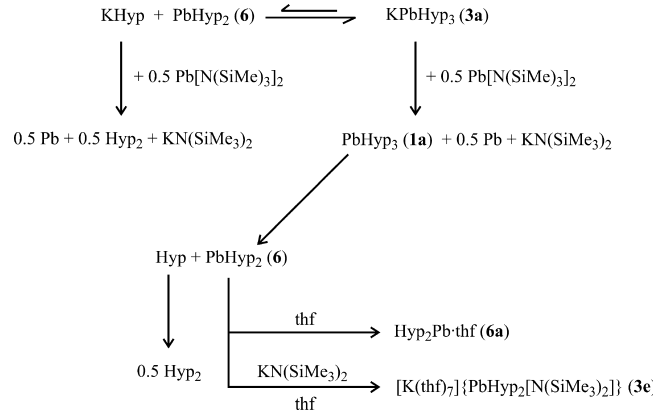

separated from the much better soluble tetrelanides, $E(OC_6H_3$-^{t}Bu$_2$-2,6)$_2$ for most cases is the better choice.[11] For plumbanides even the 2,6-di-*tert*-butylphenol itself was found to be a suitable oxidant, though here protolysis of E−Si bonds has been detected as a side-reaction.[19]

The yields of homoleptic tetryl radicals (series **1** and **2**) obtained by oxidation of the homoleptic tetrelanides (series **3** and **4**) are good in most cases but far from quantitative (according to NMR spectra of the reaction mixtures). Several diamagnetic compounds, most of them still unidentified, can be detected as side-products by NMR spectroscopy and sometimes prevent the isolation of the tetryl radical. Trihypersilylplumbyl •$PbHyp_3$ (**1a**) is only formed in a maximum yield of about 20% since most of the introduced plumbylene **6** was recovered as the thf-adduct Hyp_2Pb•thf (**6a**, Figure 6) and the heteroleptic plumbanide **3f**. As mentioned above and depicted in Scheme 3, the introduced potassium trihypersilylplumbanide (**3a**) is most probably present in an equilibrium mixture with KHyp and **6**. Therefore, not only **3a** is oxidized to the desired plumbyl radical **1a**, but also (or preferably) KHyp is oxidized to yield the octasilane Hyp_2. By detracting KHyp from the equilibrium, **6** is formed and precipitates as thf-adduct **6a** in the presence of tetrahydrofuran at lower temperatures or as plumbanide **3f** by reaction with $KN(SiMe_3)_2$ which in turn has been formed as side-product from the metathesis of $Pb[N(SiMe_3)_3]_2$ with KHyp. Further $PbHyp_2$ (**6**) may result from thermal decomposition of •$PbHyp_3$ (**1a**). EPR measurements on **1a** solutions indicate a high stationary concentration of the hypersilyl radical in solution which is in accordance with the presumed dissociation of **1a** into **6** and Hyp radicals.

Nevertheless, two plumbyl radicals, that is, **1b** and **1c**, are isolated as almost pure compounds by recrystallization from pentane or ether/*n*-pentane mixtures as green-brown crystalline solids. Crystalline stannyl (as well as silyl and germyl) radicals had already been reported very recently for slightly different substitution patterns by Sekiguchi et al.[2b] Here, further species could be generated (Table 4) of which

(19) At this moment we do not know whether the oxidation of **3b** by 2,6-di-*tert*-butylphenol proceeds via single-electron transfer or via the intermediate formation of the plumbane $HPbEbt_3$ and a subsequent thermal induced Pb−H bond fission.

(20) Klinkhammer, K. W. *Chem. Eur. J.* **1997**, *3*, 1418.

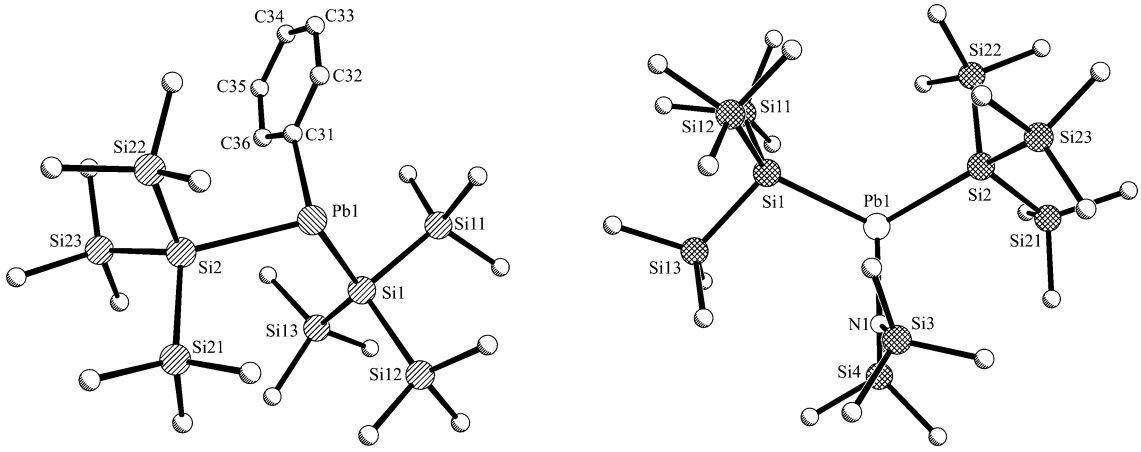

3e **3f**

Figure 3. Structures of the anions of the alkali metal plumbanides **3e** and **3f**. The counter cations have been omitted for clarity. Selected bond lengths and angles are given in [Å, deg]. $[Li(thf)_4][PbPhHyp_2]$ (**3e**): cation: Li−O (av.) anion: Pb1−Si1 2.7664(14), Pb1−Si2 274.81(12), Pb1−C31 2.324(4), Si1−Pb1−Si2 111.5(9), Si1−Pb1−C11 103.8(2), Si2−Pb1−C11 104.6(2). $[K(thf)_7]\{Pb[N(SiMe_3)_2]Hyp_2\}$ (**3f**): cation: K−O1 2.861(12), K−O2 2.769(10), K1−O3 2.732(10), K1−O4 2.755(12), K1−O5 2.753(13), K1−O6 2.846(12), K1−O7 2.755(12); anion: Pb1−Si1 2.872(3), Pb1−Si2 2.819(3), Pb1−N1 2.377(8), Si1−Pb1−Si2 111.5(9), Si1−Pb1−N1 103.8(2), Si2−Pb1−N1 104.6(2).

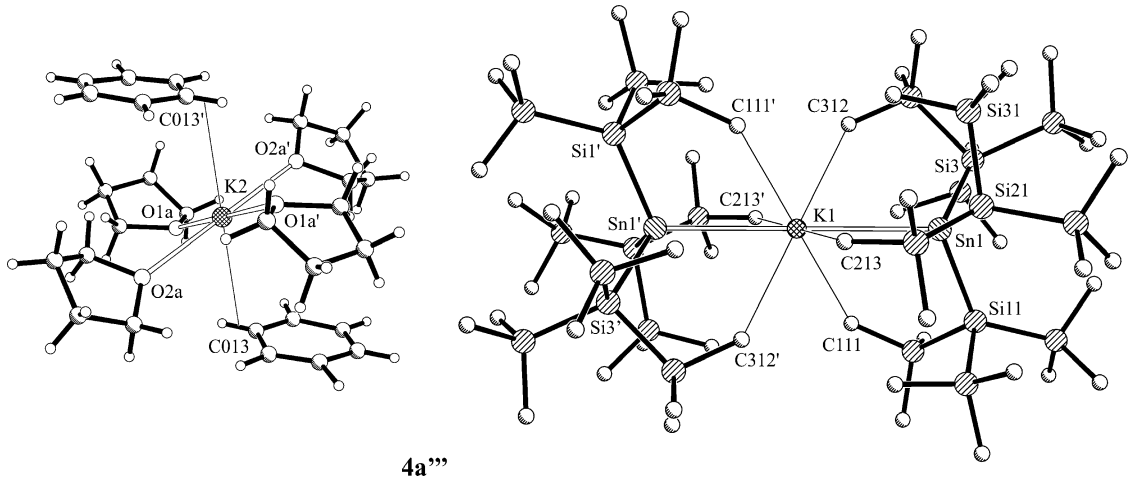

4a‴

Figure 4. Structure of the ate-complex $[K(thf)_4(benzene)_2][K(SnHyp_3)_2]$ (**4a‴**) in the crystal. Selected bond lengths and angles are given in [Å, deg]. Cation: K2−O (av.) 2.67, K2−C013 3.215(3); anion: K1−Sn1 3.7202(1), K1−Sn1−Si1 110.85 (1), K1−Sn1−Si2 110.15(1), K1−Sn1−Si3 110.04(1), Sn1−Si1 2.7222(4), Sn1−Si2 2.7301(4), Sn1−Si3 2.7283(4).

$\bullet SnHyp_3$ (**2a**) and $\bullet SnIbt_3$ (**2c**) are isolated in high yields as brown and orange-yellow crystalline materials, respectively. The plumbyl radical $\bullet PbHyp_3$ (**1a**) is formed as side-product only but could be characterized unambiguously by EPR experiments. $\bullet SnEbt_3$ (**2b**) had also been synthesized but refused to crystallize from the obtained orange-yellow oily mixture and could therefore not be separated from diamagnetic contaminations. A notable side-product from the synthesis of **2c** is the hexastannaprismane Sn_6Ibt_6 (**7**, Figure 6). It was found in small amounts as very small black crystals embedded into the large orange-yellow specimens of radical **5** and could be identified by X-ray diffraction. Whether it is formed along the synthesis of **2c** or through its decomposition remains an open question.

Some heteroleptic tetryl radicals $RHyp_2E\bullet$ could also been generated via the oxidation of heteroleptic alkali metal salts such as $RHyp_2ELi$ (E = Sn, Pb; R = Ph, alkyl). Though to date no crystalline compound could be isolated, several species such as $PhHyp_2Pb\bullet$ (**1e**) and $EtHyp_2Pb\bullet$ (**1g**) had been identified unambiguously by their unique EPR-spectroscopic data (Table 4). A detailed description of their synthesis, their geometric and electronic structure and their analytical data will be topic of a subsequent paper.

Table 1. Structural Parameters for Selected Solvated Homoleptic Silylsubstituted Alkali Metal Tetrelanides $[Cat][E(SiR_3)_3]$ and the Potassiate **4a‴**

E	Cat		R	M−E[a]	E−Si[a]	Si−E−Si
Sn	Na(toluene)	(**4a***)[20]	Hyp	3.07	2.70	109.2−110.5
Sn	$K(C_6H_6)_2(thf)_4$	(**4a‴**)	Hyp	3.72[b]	2.73	107.9−109.1
Sn	$K(OEt_2)_3$	(**4b**)	Ebt	3.72	2.66	101.0−105.7
Sn	$Li(thf)_2$	23	Si^tBu_2Me	2.83	2.66	109.5−119.3
Sn	Li(toluene)	23	Si^tBu_2Me	2.77	2.66	108.2−119.6
Sn	$Li(thf)_3$	24	$SiMe_3$	2.87	2.57	98.4−98.9
Sn	Na(15-cr-5)	25	$SiMe_3$	3.08	2.59	98.8−99.4
Pb	$K(OEt_2)_2$	(**3a′**)	Hyp	3.69	2.83	106.0−109.3
Pb	$K(OEt_2)_2$	(**3b**)[1]	Ebt	3.59	2.72	100.2−109.5
Pb	$K(OEt_2)_2$	(**3c**)	Ibt	3.61	2.72	105.8−107.9

[a] Mean values. [b] In the anion.

Molecular Structures. Figures 2−4 show the molecular structures of some novel homoleptic and heteroleptic alkali metal tetrelanides in the solid-state. They have been prepared in either of the two ways described above, (i) by reacting a

Table 2. Structural Parameters for Heteroleptic Silylsubstituted Alkali Metal Tetrelanides [Cat][EHyp$_2$Y]

E	Cat	Y	M−E	E−Si[a]	E−X	Si−E−Si	Si−E−X[a]
Sn (**4d**)	Li(Et$_2$O)$_2$	*n*Bu	3.02	2.65	2.23	114.3	95.9
Sn 20	Cs[b] 13	CH$_2$Ph	4.19	2.68	2.24	110.2	96.4
Pb (**3d**)	Li(OEt$_2$)$_2$	*n*Bu	2.95	2.73	2.32	113.2	94.5
Pb (**3e**)	Li(OEt$_2$)$_2$	Ph	*c*	2.75	2.32	112.6	95.6
Pb (**3f**)	K(thf)$_7$	N(SiMe$_3$)$_2$	*c*	2.85	2.38	111.5	104.1

[a] Mean values. [b] Mixed stannanide/amide showing intramolecular coordination by benzyl groups. [c] Solvent-separated ions.

hydrocarbon-soluble tin or lead salt with 3 equiv of the potassium salt of a branched silane or (ii) by reacting **5** or **6** with an equimolar amounts of an alkali metal salt MY of hypersilane, of a hydrocarbon, or of an amine (Y = SiR$_3$; hydrocarbyl, NR$_2$). Most of the characterized species, for which selected structural data are given in Tables 1 and 2, have been isolated from diethyl ether or other coordinating solvents as contact-ion-pairs with an M−E bond linking the solvated cation with the stannanide or plumbanide anion (Figure 2).

For trihypersilyl substituted derivatives MEHyp$_3$ **3a** and **4b** such structural motifs are also found. The solvates (toluene)NaSnHyp$_3$ (**4a***)[20] and **3a**•2Et$_2$O (**3a′**, Figure 2) gave reasonable structural data, whereas the related salt **4a**•3Et$_2$O (**4a′**) is severely disordered and no reliable structural parameters could be derived. Solvent separated ion-pairs are present in [Li(thf)$_4$][PbPhHyp$_2$] (**3d**) and [K(thf)$_7$]-[PbHyp$_2${N(SiMe$_3$)$_2$}] (**3f**, Figure 3) as well as in the salts **3a**•6THF (**3a″**) and **4a**•6THF (**4a″**). While **3d** and **3f** have been fully characterized, the two isomorphous THF-solvates **3a″** and **4a″** show severe disorder or twinning in the crystalline state, and only a rough structural picture could be derived so far, showing that both salts consist of isolated K(thf)$_6$-cations and pyramidal EHyp$_3$-anions. However, when the crystals of **4a″** are exposed to dynamic vacuum for several hours and subsequently crystallized from benzene, very large orange crystals of a well ordered phase are isolated with the composition (thf)$_2$(benzene)KSnHyp$_3$ (**4a‴**). An X-ray diffraction experiment reveals an unexpected structure: **4a** crystallizes as a unique potassium potassiate (Figure 4). It comprises two novel structural motifs: a [K(thf)$_4$-(benzene)$_2$]$^+$ cation in which the two benzene molecules are coordinating, in a unprecedented fashion, through a C−H bond and the first structurally characterized potassiate anion, [Hyp$_3$Sn−K−SnHyp$_3$]$^-$ with linearly two-coordinate potassium. However, a closer look at the C_i-symmetric anion reveals the presence of six intramolecular agostic Me···K bonding interactions leading to K−C distances of 3.40−3.49 Å. An analogous treatment of the plumbanide **3a** did not lead to an analogous bis(plumbyl)potassiate but to an almost quantitative decomposition and the formation of KHyp, elementary lead, and the octasilane Hyp$_2$.

All M−E bonds are expected to be predominantly ionic, within the neutral contact-ion pairs of **3a′** or **4a*** as well as within the potassiate anion of **4a‴**. The M−E bond length depends on the size of the alkali metal ion M and the tetryl ion E, the coordination number of M, and the steric demand of the whole anion. Common structural features for all tetrelanide ions are pyramidal EY$_3$-skeletons, relatively long E−Si bonds and small Si−E−Si or Si−E−Y angles (Tables 1 and 2). Similar structural data had been determined for tetrelanide fragments EY$_3$ of other alkali metal derivatives of stannanes and plumbanes before and are generally attributed to the presence of a lone-pair with predominant s-character at E and E−Si or E−Y bonds with a predominant p-character of the contributing orbital at the central E-atom.[21−25]

Figure 5 displays the molecular structures of the novel structurally characterized homoleptic stannyl and plumbyl radicals **1c**, **2a**, and **2c**. From etheral solutions trihypersilylstannyl (**2a**) crystallizes together with half an equivalent of ether. In the crystal two unique molecules are present. Both exhibit a well ordered structure with an approximate (noncrystallographic) C_3-symmetry. The Si−Sn−Si angles range from 116.9−119.8°; the sum of angles of 354.2° shows that the molecules are nearly but not perfectly planar. For the related stannyl radical •Sn(SiMe^{t}Bu$_2$)$_3$ as well as for its Si- and Ge-analogues Sekiguchi reported a fully planar structure within the error of the experiment (Table 3). The Sn−Si bonds (2.648 Å) in the stannyl radical **2a** are significantly shorter than those in the respective distannene Sn$_2$Hyp$_4$ (**5**$_2$) (2.672 Å),[10] the sodium trihypersilylstannanide **4a*** (2.70 Å),[20] and the potassium potassiate **4a‴** (2.726 Å). As one would expect, this finding may indicate a larger contribution of Sn 5s orbitals to the Sn−Si bonds in the radicals **2a** and **2c** than in the distannene (**5**)$_2$ or than the stannanide anions of **4a** and**4a***. While •SnIbt$_3$ (**2c**) with 2.625 Å (av.) has Sn−Si bond lengths similar to those found in the radical •Sn(SiMe^{t}Bu$_2$)$_3$ (2.618 Å),[2] the Sn−Si bonds in **2a** are slightly elongated owing to the greater bulkiness of the hypersilyl substituent as compared to the Me^{t}Bu$_2$Si group. The structural data of **2c** are unfortunately biased by disorder such that the Si−Sn−Si bond angles are less well defined. The mean value for the major orientation is 118.0°. A remarkable difference between the solid-state structure of radical **2c** and the structures of the other tin and lead radicals is its significant deviation from C_3-symmetry (which is not reflected in the EPR spectra of the frozen solutions, however). While in all other stannyl radicals the substituents are positioned paddle-wheel-like, in **2c** two Ibt-substituents are oriented in such a way that their less sterically demanding parts, the ^{i}Pr-groups, face each other, thus allowing for a small Si2−Sn1−Si3 angle of 106.7°: As a consequence, two Ibt-groups approach each other via their bulkiest parts, leading to an Si1−Sn1−Si3 angle of 131.5°.

The related novel plumbyl radical •PbIbt$_3$ (**1c**) is also paddle-wheel-shaped and expectedly exhibits somewhat longer Pb−Si bonds (2.68 Å) than the less sterically hindered

(21) Reed, D.; Stalke, D.; Wright, D. S. *Angew. Chem., Int. Ed. Engl.* **1991**, *30*, 1459.
(22) Armstrong, D. R.; Davidson, M. G.; Moncrieff, D.; Stalke, D.; Wright, D. S. *Chem. Commun.* **1992**, 1413.
(23) Fukawa, T.; Nakamoto, M.; Lee, V. Ya.; Sekiguchi, A. *Organometallics* **2004**, *23*, 2376.
(24) Cardin, C. J.; Cardin, D. J.; Clegg, W.; Coles, S. J.; Constantine, S. P.; Rowe, J. R.; Teat, S. J. *J. Organomet. Chem.* **1999**, *573*, 96.
(25) Fischer, R.; Baumgartner, J.; Marschner, C.; Uhlig, F. *Inorg. Chim. Acta* **2005**, *358*, 3174.

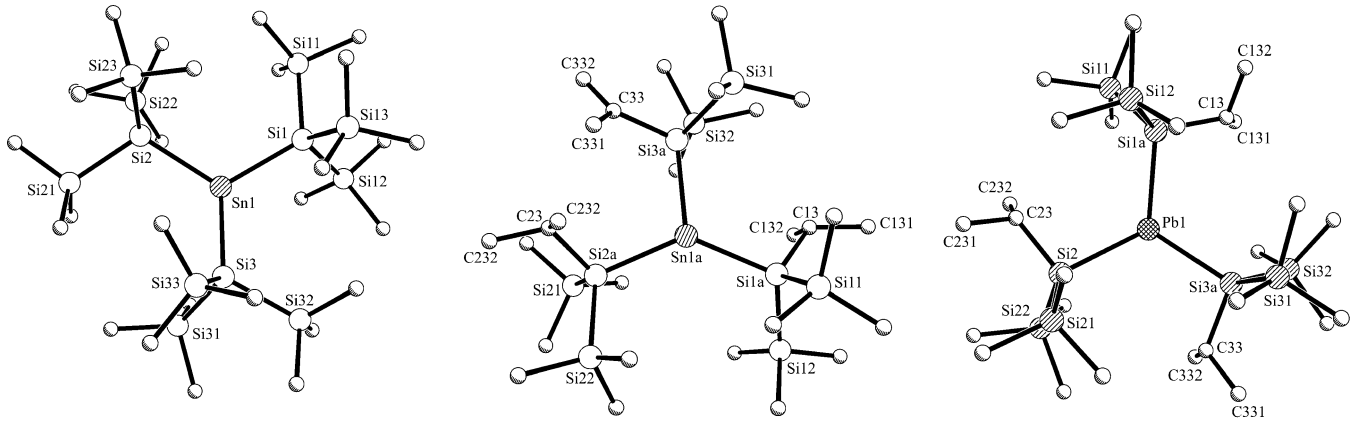

2a **2c** **1c**

Figure 5. Molecular structures of some of the radicals in the crystal. Selected bond lengths and angles are given in [Å, deg]. •$SnHyp_3$ **2a**: Sn1−Si1 2.6523(12), Sn−Si2 2.6355(13), 2.6486(13), Si1−Sn1−Si2 116.93(4), Si1−Sn1−Si3 119.80(4), Si2−Sn1−Si3 117.51(4). •$SnIbt_3$ **2c**: Sn1a−Si2a 2.607(9), Sn1a−Si1a 2.618(10), Sn1a−Si3a 2.621(7), Si2a−Sn1a−Si1a 131.5(3), Si2a−Sn1a−Si3a 106.7(3), Si1a−Sn1a−Si3a 115.7(3). •$PbIbt_3$ **1c**: Pb1−Si1a 2.678(5), Pb1−Si2 2.679(2), Pb1−Si3a 2.676(2), Si1a−Pb1−Si2 117.34(12), Si1a−Pb1-Si3a 115.9(2), Si2−Pb1−Si3a 117.1(2).

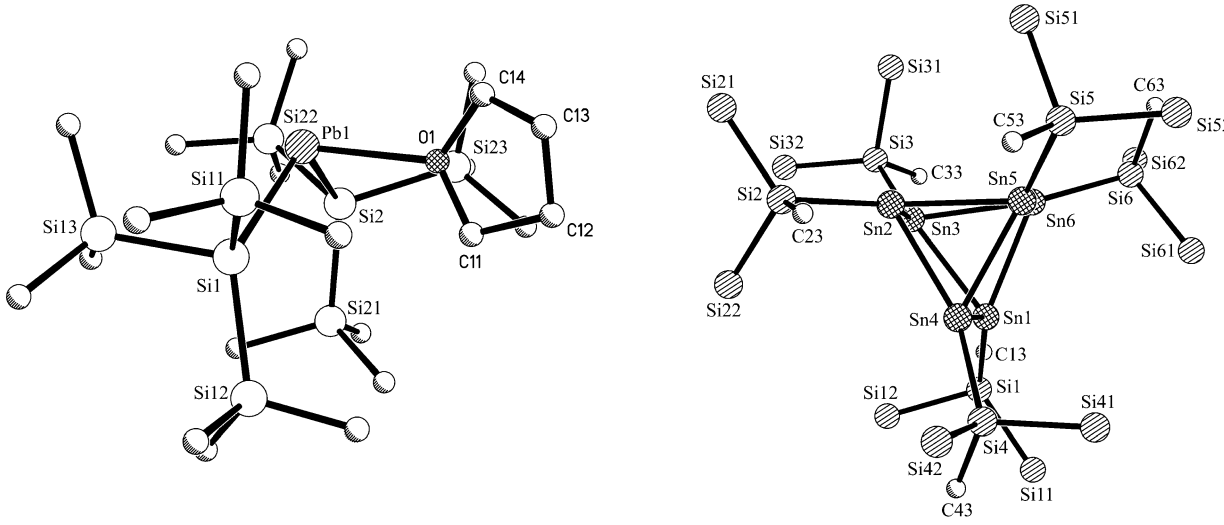

6a **7**

Figure 6. Molecular structures of the THF-adduct **6a** and hexastannaprismane **7** in the crystal. Selected bond lengths and angles are given in [Å, deg]. Hyp_2Pb•THF (**6a**): Pb1−O1 2.531(5), Pb−Si1 2.743(2), Pb−Si2 2.7318(15), Si1−Pb1−Si2 112.89(5), Si1−Pb1−O1 93.32(12), Si2−Pb1−O1 96.30(13). Sn_6Ibt_6 (**7**): All methyl groups (two on each carbon and three on each silicon) as well as all remaining hydrogen atoms had been omitted for clarity. Sn1−Sn4 2.827(10), Sn1−Sn6 2.851(10), Sn1−Sn3 2.866(9), Sn2−Sn3 2.811(10), Sn2−Sn4 2.853(9), Sn2−Sn5 2.850(7), Sn3−Si3 2.584(10), Sn3−Sn6 2.839(7), Sn4−Sn5 2.849(10), Sn5−Sn6 2.821(10), Sn1−Si1 2.566(10), Sn2−Si2 2.582(9), Sn4−Si4 2.586(9), Sn5−Si5 2.577(10), Sn6−Si6 2.594(9).

Table 3. Selected Structural Parameters for Silylsubstituted Tetryl Radicals ER_3 (E = Sn, Pb)

E	R	E−Si[a]	Si−E−Si	Σ(Si−E−Si)	
Sn	Hyp	2.64	116.9−119.8	354	**4a**
Sn	Ibt	2.62	106.7−131.3	354	**4c**
Sn	tBu$_2$Me	2.63	119.7−120.2	360	2b
Pb	Ebt	2.64	115.2−121.4	353	**3b**
Pb	Ibt	2.68	115.9−117.1	350	**3c**

[a] Mean values.

•$PbEbt_3$ (**1b**, 2.65 Å).[1] In these plumbyl radicals a trend similar to that in the stannyl radicals is observed: the Pb−Si bonds are significantly shorter than for silylsubstituted plumbandiyls such as **6** (2.702 Å) and $Pb[Si(SiMe_3)_2(Si^iPr_3)]_2$ (2.745 Å) or the related plumbanide **3a′** (2.715 Å). Unfortunately, the structural parameters are again biased by disorder. However, the derived sums of the Si−Pb−Si angles of 350° and 355° for the two refined orientations are very similar to the respective value for •$PbEbt_3$ **1b** (353°) and again prove a non-planar structure for this plumbyl radical.

Two side-products occurring during the synthesis of the tetryl radicals **1a** and **2c** could also be structurally characterized and are depicted in Figure 6. The right-hand side of Figure 6 displays the molecular structure of the hexastannaprismane **7** derived from diffraction data on very small black crystals that were embedded into larger orange crystals of the stannyl radical **2c**. While the Sn_6Si_6-scaffold is very similar compared to the related hexastannaprismane, $(^tBu_3Si)_6Sn_6$ that was structurally characterized by Wiberg some years ago,[26] the Sn−Sn and Si−Si bonds in **7** as compared to $(^tBu_3Si)_6Sn_6$ are shorter by 7 and 13 pm, respectively, because of the less bulky substituents.

Figure 6 (left) shows the molecular structure of the tetrahydrofuran-adduct **6a**, which is formed alongside the

Table 4. EPR Data of Selected Mononuclear Tetryl Radicals ER_3

	E	R	g_{iso} (293 K)	a_{iso} (293 K)/mT	g	A/mT
1a[a]	Pb	Hyp	2.089	(^{207}Pb): 84.3	[2.237, 2.213, 1.893]	(^{207}Pb): [42.0, 44.0, 175]
1b[a]	Pb	SiEt(SiMe$_3$)$_2$	2.105	(^{207}Pb): 50.6	[2.246, 2.245, 1.888]	(^{207}Pb): [13.9, 15.3, 144.2]
1c[a]	Pb	Si^{i}Pr(SiMe$_3$)$_2$	2.097	(^{207}Pb): 79.1		
1g[a]	Pb	Hyp (2x), Et	2.055	(^{207}Pb): 125.8	[2.226, 2.079, 1.890]	(^{207}Pb): [104.0, 142.0, 147.0]
1e	Pb	Hyp (2x), Ph	2.043	(^{207}Pb): 124.3	[2.255, 1.998, 1.894]	
24	Pb	Me	2.039 (77K)		[2.106, 2.097, 1.914]	(^{207}Pb): [115, 115, 324]
2a[a]	Sn	Hyp	2.042	(^{117}Sn): 59.8 (^{119}Sn): 62.4	[2.074, 2.074, 1.991]	(^{117}Sn): [36.3, 36.3, 107.8] (^{119}Sn): [38.0, 38.0, 112.5]
2b[a]	Sn	Si^{i}Pr(SiMe$_3$)$_2$	2.055	(^{117}Sn): 39.1 (^{119}Sn): 41.6		
2c[a]	Sn	SiEt(SiMe$_3$)$_2$	2.053	(^{117}Sn): 37.7 (^{119}Sn): 39.8	[2.080, 2.079, 1.985]	(^{117}Sn): [18.8, 20.9, 90.2] (^{119}Sn): [20.9, 24.0, 94.4]
24	Sn	Me	2.016 (77K)		[2.030, 2.024, 1.995]	(^{117}Sn): [133.2, 119.2, 206.7] (^{119}Sn): [141.5, 126.2, 215.7]
5a	Sn	CH(SiMe$_3$)$_2$	2.009	(^{117}Sn): 169.8 (^{119}Sn): 177.6	[2.016, 2.016, 1.994]	
32	Sn	Tar[b]	2.001	(^{117}Sn): 175.6 (^{119}Sn): 182.7		
33	Sn	H		3800	[2.024, 2.024, 2.015]	
5d	Sn	N(SiMe$_3$)$_2$	1.991	(^{117}Sn): 317.6 (^{119}Sn): 342.6		
2b	Sn	SitBu$_2$Me	2.048	($^{117/119}$Sn): 32.9		
2a	Ge	SitBu$_2$Me	2.023	(^{73}Ge): 2.0		
32	Ge	Tar[b]	2.005	(^{73}Ge): 8.5		
2a	Si	SitBu$_2$Me	2.006	(^{29}Si): 5.8		

[a] The isotropic values g_{iso} and a_{iso} from simulations of the solution CW EPR spectra at 293 K; g- and A-tensors from simulations of frozen solution spectra. Margins of error are $\Delta g = \pm 0.0002$; $\Delta A = \pm 0.1$ mT. [b] Tar = C$_6$H^{t}Bu-2-Me$_3$-4,5,6.

preparation of **1a** and may be independently prepared as blue-green crystals in quantitative yields by addition of tetrahydrofuran to a solution of **6** in *n*-pentane and subsequent crystallization at −60 °C. As expected, **6a** possesses a pronounced pyramidal Si_2PbO-scaffold (sum of angles around Pb: 302.5°). The length of the Pb−O dative bond (2.53 Å) is somewhat longer than in the thf-adduct of the more polar lead thiolate Pb{S[C$_6$H$_2$(CF$_3$)$_3$-2,4,6]$_2$ (2.50 Å)[27] but significantly shorter than in the extremely sterically overcrowded thf-adduct of the molybdylplumbylene Pb[Mo(η-C$_5$Me$_5$)(CO)$_3$]$_2$ (2.75 Å).[28]

EPR Spectroscopy. Figure 7 displays CW EPR spectra of the four compounds **1a**, **1b**, **2a**, and **2c** at room temperature (293K), while Figure 8 depicts the echo-detected, field-swept EPR spectra at low temperature (20K). Overlaid in red we also present spectral simulations including the hyperfine pattern expected from the magnetically active isotopes ^{207}Pb (I = 1/2, natural abundance of 22.1%) and ^{117}Sn (I = 1/2, natural abundance of 7.5%) as well as ^{119}Sn (I = 1/2, natural abundance of 8.6%).

Room-Temperature CW EPR Spectra. When measuring solutions of the four compounds in alkanes at room temperature (293 K), the usually orientation-dependent (i.e., anisotropic, tensorial) magnetic interactions of the electron spin with the magnetic field (the electron-Zeeman interaction) and the interaction of the electron spin with magnetic nuclear spins (the hyperfine (hf) interaction) are averaged to their isotropic, scalar values g_{iso} and a_{iso}.[29] While the spectra of the stannyl radicals **2a** and **2c** are shown in panels a and b of Figure 7, spectra of the plumbyl radicals **1a** and **1b** are presented in panels c and d of Figure 7, respectively. All spectra in Figure 7 show the same general pattern and possess a strong main signal from the radical centered at nonmagnetic Pb- and Sn-isotopes, as well as peak patterns that reflect hyperfine splitting from the magnetically active isotopes. The hyperfine coupling constants that were extracted from the spectral simulations are summarized in Table 4. In general, the isotropic g-values g_{iso} can be seen as the fingerprint for the individual radical species, and the isotropic hf coupling constants a_{iso} characterize the interaction between the electron spin and the nuclear spin of the magnetically active nuclei.[29] In the case of the Sn-based radicals, we find for **2a** g_{iso} = 2.042 and an a_{iso}(^{117}Sn) = 59.8 mT, a_{iso}(^{119}Sn) = 62.4 mT while **2c** shows significantly higher g- and lower a-values: g_{iso} = 2.053, a_{iso}(^{117}Sn) = 37.7 mT, a_{iso}(^{119}Sn) = 39.8 mT. As it is expected, the ratio of the hf coupling constants for the two isotopomers reflects the ratio of the respective gyromagnetic ratios γ(^{119}Sn)/γ(^{117}Sn). Because of the larger hf coupling of **2a**, in this case even the characteristic splitting pattern for the two isotopomers can be distinguished, while for **2c** the hf lines still overlap.

The lead-based radicals show g-values that deviate stronger from the free electron g-value. For **1a** we find g_{iso} = 2.089 and a_{iso}(^{207}Pb) = 84.3 mT, while **1b**, as is the case for the respective stannyl radical, shows a higher g- and a lower a-value: g_{iso} = 2.105, a_{iso}(^{207}Pb) = 50.6 mT. When exchanging the central Sn^{III} (fifth period in the periodic table of elements) with the heavier congener Pb^{III} (sixth period), the larger contribution of the spin−orbit coupling is responsible for an even greater deviation of the plumbyl radicals' g-values from the free electron g-value g_e = 2.0023.

(26) Wiberg, N.; Lerner, H.-W.; Nöth, H.; Ponikwar, W. *Angew. Chem., Int. Ed.* **1999**, *38*, 1103.
(27) Labahn, D.; Brooker, S.; Sheldrick, G. M.; Roesky, H. W. *Z. Anorg. Allg. Chem.* **1992**, *610*, 163.
(28) Hitchcock, P. B.; Lappert, M. F.; Michalczyk, M. J. *J. Chem. Soc., Dalton Trans.* **1987**, 2635.
(29) Atherton, N. M. *Principles of Electron Spin Resonance*; Ellis Horwood: New York, 1993.

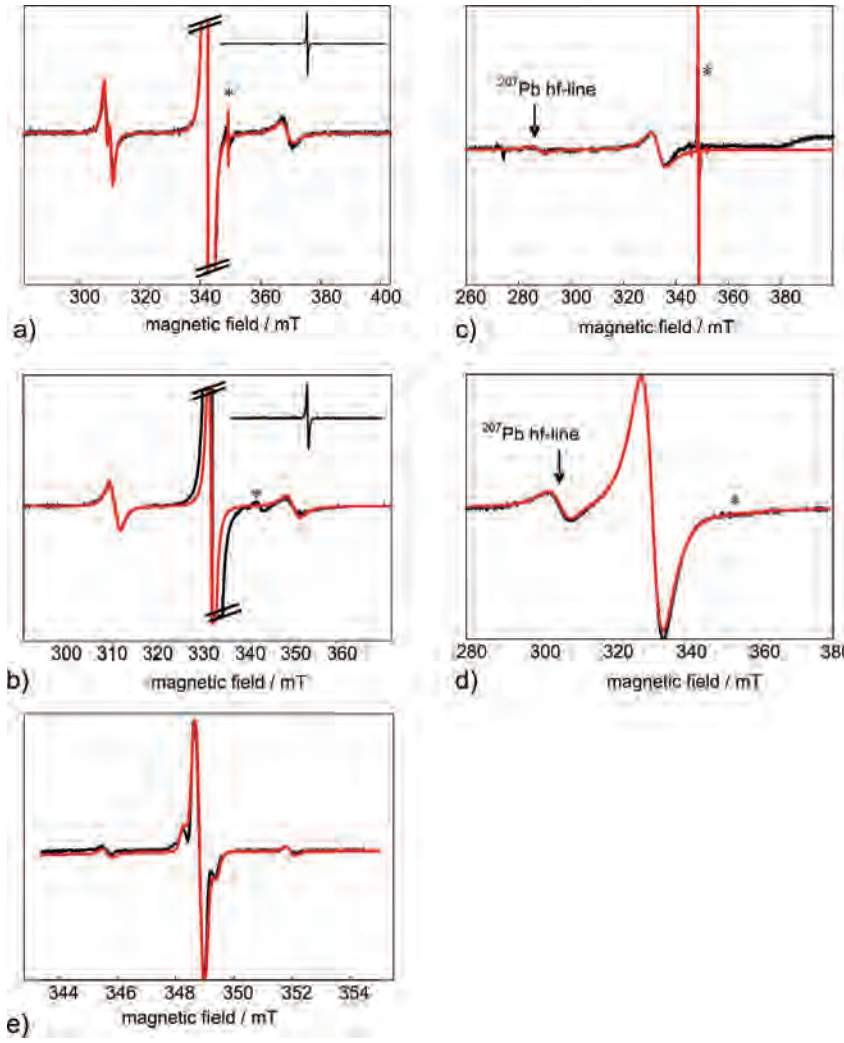

Figure 7. CW EPR spectra of the radicals depicted in Figure 1 in mixtures of *n*-pentane and *n*-hexane at 273 K. All experimental spectra (black) are overlaid with spectral simulations (red). (a) •$SnHyp_3$ (**2a**), the inset shows the full spectrum; the enlarged part shows the detailed hyperfine splitting pattern; (b) •$SnIbt_3$ (**2c**), the inset shows the full spectrum; the enlarged part shows the detailed hyperfine splitting pattern; (c) •$PbHyp_3$ (**1a**), (d) •$PbEbt_3$ (**1b**); the respective lines marked with an asterisk are from a stationary concentration of a silyl-based radical, which for **1a** is displayed in detail in (e).

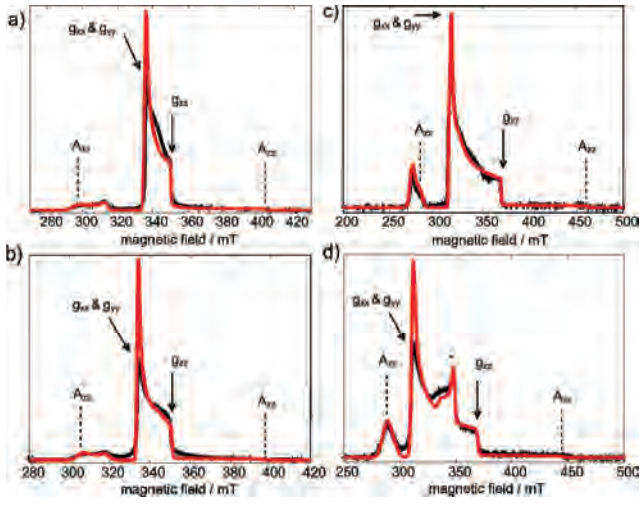

Figure 8. Echo-detected, field swept EPR spectra of the radicals depicted in Figure 1 in mixtures of *n*-pentane and *n*-heptane at 20 K. All experimental spectra (black) are overlaid with spectral simulations (red). The approximate *g*-tensor element positions are marked with arrows, and the largest hf coupling tensor element A_{zz} is marked by dashed lines. (a) **2a**; (b) **2c**; (c) **1a**; (d) **1b**; the asterisk marks features from an unknown impurity or paramagnetic side product.

Note that two heteroleptic plumbyl radicals **1e** and **1g** for which we report *g*- and *A*-values in this work (spectra not shown; for the values see Table 4) also have markedly smaller *g*-values and significantly larger a_{iso}-values as compared to the homoleptic Pb-based radicals.

One interesting feature in Figure 7 is the asymmetric broadening of the hyperfine lines, which in the case of the two plumbyl radicals (see Figure 7c,d) even leads to such a strong broadening that the high-field line is not distinguishable from the background signal any more. Note that the difficulties in observing the high-field line manifolds of plumbyl radicals have led to some confusion about the purity of the materials in the initial report on these materials.[1] This effect can be understood when considering the modulation of the anisotropic electron Zeeman and hf interactions by the rotational motion. It can be accounted for by using a slow motion model for spectral simulations that is based on solving the stochastic Liouville equation (simulations shown in Figure 7).[16,29] We find that a characteristic rotational correlation time of $\tau_c \approx 1.3 \cdot 10^{-10}$ s can nicely reproduce the hf splitting and intensity pattern for the two lead-based

radicals, while we find significantly faster rotation with $\tau_c \approx 6.3 \times 10^{-11}$ s for the two tin-based radicals (all measured in the same solvent mixture). This apparent slowdown in the rotational motion when the central atom Sn is replaced with the larger and much heavier Pb can be attributed to the overall increased mass of the plumbyl radical molecules.

Note that in the spectra of **1a** and **2a**, and to a lesser degree also in the spectra of **1b** and **2c**, additional narrow lines corresponding to significant amounts of a radical species with a *g*-value of 2.0058 rather close to the value of a free electron and a characteristic hyperfine splitting pattern are observed (marked with asterisks in Figure 7. This five-line pattern is shown in Figure 7e and can be described as one intense central line and two pairs of hyperfine lines. We assign this specific EPR pattern to a silicon-based decay product of our stannyl and plumbyl radicals, the hypersilyl ligand radical $\bullet Si(SiMe_3)_3$ (or $\bullet Si^iPr(SiMe_3)_2$, and $\bullet SiEt(SiMe_3)_2$ in the case of $\bullet SnIbt_3$ and $\bullet PbEbt_3$, respectively). The strong central line stems from the electron spins located on the almost 96% of Si nuclei that are not magnetic and therefore do not lead to a hyperfine splitting. The *g*-value of 2.0058 and the observed hyperfine-splittings of 6.25 mT and 0.86 mT (due to the 4.2% ^{29}Si nuclei) are in reasonable agreement to the values of branched silyl radicals found in literature.[4,30]

As can be expected, the difference of the splitting patterns between the hypersilyl ligand radical and the ligand radicals derived from $\bullet EIbt_3$ and $\bullet EEbt_3$ lies mainly in the intensity-ratios of the ^{29}Si hyperfine lines. The splittings (i.e., position of the lines) are virtually identical. From the ratio of the isotropic hyperfine splitting constants it is obvious that in the hypersilyl ligand radical the electron spin is mainly located on the one Si-atom with the largest hyperfine splitting ($\rho_s \sim 0.841$) but is delocalized to a certain degree onto the three Si atoms of the trimethylsilyl groups ($\rho_s \sim 0.053$ for each).

We can quantify the concentration of the hypersilyl radical decay product in solutions of $PbHyp_3$ by measuring the double integral of the CW EPR spectral excerpt that contains the Si-based radical signal. The double integral is a direct measure of the number of electron spins. We find that the concentration of the Si-based radical remains constant within the precision of the experiment for several hours at room temperature (or elevated temperatures) while the decay of the Pb-based radical is apparent. This leads to the conclusion that the concentration of the hypersilyl radical is a stationary intermediate in the decomposition reaction of $\bullet PbHyp_3$. The fact that a stationary concentration of the hypersilyl radical builds up in a highly reproducible manner opens up new possibilities for use of the radical as a clean silylating agent. Note that despite the highly intense central silyl-radical line, the overall contribution to the concentration of electron spins (i.e., the double integral) was never more than 1.5%.

Low-Temperature EPR Spectra. In frozen solution the anisotropies of the *g*- and hf (*A*-) tensors of the radicals are not averaged out any more and now dominate the spectra. The echo-detected EPR spectra of the four radicals at 20 K along with powder-averaged EPR spectral simulations are presented in Figure 8. The *g*- and *A*-tensor elements are summarized in Table 4. All spectra consist of one main spectral component that is typical for a radical with an approximately axial *g*-tensor ($g_{xx} \approx g_{yy} \neq g_{zz}$) and less intense pattern spreading out to lower and higher magnetic field values that stem from the hyperfine coupling to the magnetic nuclei in the respective isotopomers. In Figure 8 we also indicate the approximate position of the g_{xx}/g_{yy} and g_{zz} tensor elements in the isotopomers that have no magnetically active Sn and Pb nuclei.

Our simulations clearly show that also the hf tensor for homoleptic radicals is nearly axial ($A_{xx} \approx A_{yy} \neq A_{zz}$) with $A_{zz} \gg A_{xx}/A_{yy}$, and in Figure 8 the splitting from the A_{zz}-tensor element is marked by dashed lines. For both cases, tin and lead, the hypersilyl compounds display the significantly larger hyperfine coupling (a_{iso} as well as all the *A*-tensor elements) when compared with the radicals having unsymmetrically substituted ligands (**2c** and **1b**, respectively). In addition, the heteroleptic lead-based radicals **1g** and **1d** clearly have an orthorhombic low-temperature EPR-spectrum (see Table 4, data not shown, $g_{xx} \neq g_{yy} \neq g_{zz}$) and ($A_{xx} \neq A_{yy} \neq A_{zz}$) with *g*-values smaller than those of the homoleptic radicals and hyperfine values significantly larger than those of the homoleptic radicals. There are only few reports in the literature on EPR investigations of simple mononuclear triorganylstannyl and triorganylplumbyl radicals such as $\bullet PbMe_3$, $\bullet SnMe_3$, or $\bullet Sn{\it i}Bu_3$.[31] Two general trends can nonetheless be easily recognized going from hydrogen via organyl to silyl substitution (Table 4): (i) *g*-values increase and (ii) hyperfine-coupling constants markedly decrease. It becomes obvious that those trends have to be attributed mainly to differences in electronic properties of the substituents and only to a lesser extent to different steric demands of the substituents (vide infra).

Electronic and Geometric Structure and the Dynamics of the Radicals. The information gained from the EPR spectra in both, fluid solution at room temperature and in frozen solution at 20 K, together with structural data from X-ray diffraction give unique insight into these new compounds. Conclusions can be drawn not only about the electronic structure but also about the geometric structure and the dynamic properties of the persistent or stable heavy main group element radicals. Some of the generated radicals, which we have extensively characterized by EPR measurements, could also be obtained as suitable crystals for X-ray diffraction, others were obtained as microcrystalline powders

(30) (a) Bennett, S. W.; Eaborn, C.; Hudson, A.; Jackson, R. A.; Root, K. D. J. *J. Chem. Soc. A* **1970**, 348–351. (b) Azinovic, D.; Bravo-Zhivotovskii, D.; Bendikov, M.; Apeloig, Y.; Tumanskii, B.; Veprek, S. *Chem. Phys. Lett.* **2003**, *374*, 257–263.

(31) (a) Bennett, J. E.; Howard, J. A. *Chem. Phys. Lett.* **1972**, *15*, 322–324. (b) Booth, R. J.; Fieldhouse, S. A.; Symons, M. C. R. *J. Chem. Soc., Dalton Trans.* **1976**, 1506–1515.

(32) Della Bona, M. A.; Cassani, M. C.; Keates, J. M.; Lawless, G. A.; Lappert, M. F.; Stürmann, M.; Weidenbruch, M. *J. Chem. Soc., Dalton Trans.* **1998**, 1187.

(33) Morehouse, R. L.; Christiansen, J. J.; Gordy, W. *J. Chem. Phys.* **1966**, *45*, 1751.

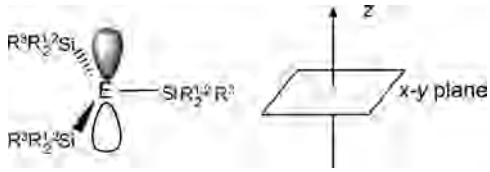

Figure 9. Scheme of the proposed axial *g*-or *A*-tensor frame (right-hand side) and main contribution to the SOMO bearing the unpaired electron (left-hand side).

or as viscous oils only (vide supra). As mentioned before, the structural data derived for crystalline species are unfortunately frequently biased by disordering in the solid state. Nevertheless, the diffraction data revealed that all silyl substituted tetryl radicals exhibit a nearly but not fully planar structure, which is also consistent with the nearly axial *g*- and *A*-tensors found for the radicals and is schematically displayed in Figure 9. Surprisingly, among the tin-based radicals the most pronounced pyramidalization is found for trihypersilyltin (**2a**) although the hypersilyl group is the bulkiest substituent used and should therefore lead to less pyramidalization. Unfortunately, because of its lower stability we were not able to get crystals for its lead analogue **1a**. The EPR data (in particular the larger isotropic hf coupling constants) for both **1a** and **2a** indicate a higher degree of pyramidalization than for the other plumbyl and stannyl radicals.

As pointed out by Sekiguchi et al. crowding is not the only reason for the almost planar structures of silyl substituted group 14 radicals. Hyperconjugation, that is, delocalization of spin density into the antibonding σ^*(Si−Si)-orbitals, also has to be taken into account. Detailed quantum-chemical analyses are lacking, however, and are on the agenda in our groups. A further typical structural feature of all tetryl radicals ER_3 is the comparably short E−Si bond found in the solid-state (vide supra) being markedly shorter than that determined for the related tetrelandiyls ER_2 and close to those observed in stress-free tetrelanes ER_4. This can be explained by assuming a significantly higher contribution of the contracted 6s orbital of lead in bonding to the silyl substituents than in the related plumbandiyls, in which this orbital predominantly contributes to the lone-pair.

The EPR measurements can add further information about the geometric structure of the radicals. As displayed in Figure 9, a fully planar group 14 radical should have a 5p (tin) or 6p (lead) singly occupied molecular orbital (SOMO) bearing the unpaired electron and the overall hybridization should be sp^2, that is, the three ligands should be bound via such sp^2 hybrid orbitals. In this ideal sp^2-hybridization case, except for minor spin polarization effects (polarization of the electrons in the closed shells),[22] the isotropic hf coupling should be zero (or have only small values), since the main contribution to a_{iso} comes from unpaired spin density in s-(σ-)type orbitals and the unpaired electron resides in a p_z-orbital. Two factors lead to a significant a_{iso} in fluid solution for our tin and lead tetryl radicals: (i) an intrinsic pyramidalization, probably as an effect of the different ligands, and (ii) the structure is dynamic and even a perfectly planar molecule will oscillate along the molecular *z*-direction such that a dynamic pyramidalization takes place. The static pyramidalization can be approximated when inspecting the *A*-tensor elements. All four investigated tetryl radicals have an *A*-tensor with an A_{zz}-value that is much larger than the respective *x*-and *y*-values A_{xx} and A_{yy}, which are (almost) equal, that is, the tensor is axial as depicted in Figure 9. The hypersilyl compounds **1a** and **2a** do not only have a larger a_{iso} but also the *A*-tensor elements along all three directions are larger than in the respective other radical (e.g., for the plumbyl radicals: **1a**, [42.0 44.0 175] mT vs **1b**, [13.9 15.3 144.2] mT). This is fully consistent with a larger pyramidal deviation from planarity in the case of the hypersilyl tetryl radicals also in frozen solution.

The most pronounced pyramidalization can be found for the Pb-based heteroleptic radicals **1e** and **1g**, which is due to the size difference for the individual ligands (two hypersilyl ligand and one ethyl or phenyl ligand, respectively). This is expected and leads to a much stronger s-type character for the orbital bearing the unpaired electron, which in turn leads to a much larger isotropic contribution to the hyperfine coupling (see Table 4). Also note that the *g*-values for **1e** and **1g** are much closer to the *g*-value reported for $PbMe_3$.

At room temperature and if light is excluded, the stannyl radicals **2a**−**2c** show only a very slow decomposition. Although small amounts of branched silyl radicals are always detected in solution, their decay rates could not be determined so far; half-life times of at least several weeks at room temperature can, however, be estimated. All plumbyl radicals synthesized show half-life times of a few hours at room temperature. While in the case of trihypersilyl plumbyl **1a** the corresponding plumbandiyl **6** and the octasilane Hyp_2 are detected as main products, the less hindered **1b** cleanly decomposes within a few days giving elementary lead and $PbEbt_4$. No intermediate and almost no side-products are found. Most probably, the corresponding plumbandiyl $PbEbt_2$ is the first intermediate, since the rate-determining step is first order in **1b** and the activation barrier had been measured to be about 100 KJ mol^{-1}.[1] This would be fully in accordance with a Pb−Si bond fission as the first and rate-determining step. The generated Ebt radical which could be detected by EPR to be present in a stationary concentration may then quickly react with remaining **1b** to produce the plumbane $PbEbt_4$. The facts that hardly any side-products are observed and that the rate for the formation of $PbEbt_4$ is equal to the rate of the decomposition of **1b** within the experimental errors leads to the conclusion that the plumbandiyl $PbEbt_2$ is not stable under these conditions, but disproportionates very quickly to give further amount of elementary Pb and $PbEbt_4$. Oligonuclear plumbanes or diplumbenes are very probable intermediates and trapping experiments are in our hands.

Conclusions and Outlook

We were able to synthesize a series of homoleptic and heteroleptic alkali metal stannanides and plumbanides, and via subsequent oxidation got access to further persistent mononuclear tin and lead radicals, respectively, showing either a homoleptic or a heteroleptic substitution pattern.

While the homoleptic tetryl radicals **1b**, **1c**, **2a**, and **2c** could be isolated as crystalline compounds, others such as the homoleptic **1a** and **2b** or the heteroleptic species **1e** and **1g** could only be characterized by EPR experiments. EPR-spectroscopic studies enable us to draw conclusions about the electronic and geometric structure as well as the dynamics of these novel, molecular persistent tin and lead tetryl radicals, even for those cases where the radical is not stable or clean enough to be isolated as a pure compound. As indicated in the X-ray diffraction results on some of the radicals, the structures are best described as almost planar with varying small pyramidal distortion (flexible pyramidal). Interestingly, we find that the bulkiest ligand, hypersilyl, shows the largest deviation from planarity for both cases, stannyl and plumbyl radicals. This may possibly be due either to differences in ligand-ligand interactions among the C_3-symmetric hypersilyl groups compared with Ebt and Ibt groups having approximate C_s symmetry or to a different extent of hyperconjugation with the lone-pair on E. For a more detailed discussion of the radical structure, more sophisticated pulse EPR methods are necessary. Currently, we study the electronic structure of the radicals by measuring the hyperfine coupling to the ligand protons and silicon nuclei by means of pulse electron−nuclear double resonance (ENDOR) and methods based on electron spin echo envelope modulation (ESEEM, HYSCORE). These methods give detailed information about small hyperfine couplings between ligands and nuclei and should help in elucidating not only the spin density distribution from the central main group element onto the ligand but also the fine details of distortion from planarity.

The clean decay of the •$PbHyp_3$ (**1a**) and •$PbEbt_3$ (**1b**) radicals in particular is of interest since its first step seems to deliver a stationary concentration of a well defined branched silyl radical, which may be useful in synthetic approaches as a clean silylating agent. Efforts toward the preparation of polymer-supported silyl substituted tetrelanides and respective tetryl radicals and thus precluding a contamination by soluble tin or lead containing side products are currently underway.

Acknowledgment. The authors thank Christian Bauer for technical support, Bernd Mathiasch for NMR measurements, and Hans Wolfgang Spiess for continuing support. This work is dedicated to the memory of Professor Nils Wiberg.

Supporting Information Available: Tables with crystal and structure refinement parameters. This material is available free of charge via the Internet at http://pubs.acs.org.

IC801198P